Spring 5-10-2016

Isothermal Titration Calorimetry Uncovers Substrate Promiscuity of Bicupin Oxalate Oxidase

Hassan Ali Rana

Isothermal Titration Calorimetry Uncovers Substrate Promiscuity of Bicupin Oxalate Oxidase

By Hassan Rana

ACKNOWLEDGEMENTS

Kennesaw State University- Department of Chemistry and Biochemistry

Ellen Moomaw, Ph.D

Daniela Tapu, Ph.D

Michael Van Dyke, Ph.D

ABSTRACT

Oxalate oxidase from *Ceriporiopsis subvermispora* (CsOxOx) is a manganese-dependent enzyme that catalyzes the oxygen-dependent oxidation of oxalate to form two moles of carbon dioxide and one mole of hydrogen peroxide. CsOxOx is the first oxalate oxidase reported to have a two beta barrel architecture (bicupin). The CsOxOx catalyzed oxidation of oxalate reaction can be monitored by coupling the product H_2O_2 to the horseradish peroxidase-catalyzed oxidation of 2,2'-azinobis-(3- ethylbenzthiazoline-6-sulphonic acid) and by membrane inlet mass spectrometry. Coupled enzyme assays often confound data interpretation. Isothermal titration calorimetry (ITC) measures heat changes that occur during a reaction. Therefore, ITC can measure reaction rates where both the substrates and products are spectrophotometrically silent and when the reaction products are unknown. In this work, we apply the multiple injection method of ITC to characterize the catalytic properties of oxalate oxidase. Steady-state kinetic constants using oxalate as the substrate determined by multiple injection ITC are comparable to those obtained by the horseradish peroxidase coupled assay and by membrane inlet mass spectrometry. Furthermore, we used this technique to identify mesoxalate as a substrate for the CsOxOx-catalyzed reaction, with kinetic parameters comparable to that of oxalate, and to identify a number of small molecule carboxylic acid compounds that also serve as substrates for the enzyme.

Table of Contents

List of Figures

List of Tables

CHAPTER 1. INTRODUCTION

Oxalate plays functional roles in plants, fungi, bacteria and animals. In high concentrations calcium oxalate crystals produce kidney stones in humans.[1] Oxalate is utilized by plants to protect against pathogens and regulate ions.[2] Certain species of soil bacteria utilize oxalate as their only carbon source (oxalotrophic) playing an important role in regulating the carbon cycle by utilizing oxalate-degrading enzymes.[3]

Oxalate-Degrading Enzymes

Oxalate-degrading enzymes expressed in certain species of plants, bacteria and fungi fall into three classes: oxalate oxidases, oxalate decarboxylases and oxalyl-CoA decarboxylases.[3] Oxalate oxidase (OxOx) is expressed by plants, whereas oxalate decarboxylase (OxDC) is expressed by bacteria and fungi.[4,5] Oxalyl-CoA decarboxylase (OXC) is utilized by oxalotrophic bacteria and plays an important role in the gastrointestinal tract of animals by consuming the oxalate that is toxic to animals.[6,7] Oxalate oxidase catalyzes the carbon-carbon bond cleavage of oxalate and produce carbon dioxide and hydrogen peroxide.[4] Oxalate decarboxylase cleaves the same carbon-carbon bond of oxalate and produces carbon dioxide and formate.[8] Oxalyl-CoA decarboxylase catalyzes the cleavage of oxalyl-CoA to formyl-CoA and carbon dioxide. Since OXC does not possess the cupin architecture and uses an unrelated reaction mechanism, it is not described further here.

Oxalate oxidase and oxalate decarboxylase are found within the cupin superfamily, which is characterized by a β-barrel domain.[9] The cupin superfamily contains diverse proteins ranging from catalytically inactive seed storage proteins and sugar-binding metal-independent proteins to metal-dependent enzymes.[9] While most enzymes in the cupin superfamily contain iron as its cofactor, others contain zinc, nickel, manganese, cobalt or copper. Oxalate oxidase and oxalate decarboxylase utilize manganese cations as a cofactors. Oxalate oxidase uses dioxygen as a substrate whereas oxalate decarboxylase requires but does not consume oxygen. All characterized plant oxalate oxidases possess a single β-barrel domain (monocupin), whereas oxalate decarboxylases expressed by fungi and soil bacteria are characterized by two β-barrel domains (bicupin), each containing a manganese ion.[10-12]

The active sites of oxalate oxidase and oxalate decarboxylase are characterized by four conserved residues (three histidines and one glutamate) coordinating the Mn centers, which exist as Mn^{2+} in the resting.[13,14] The proposed catalytic mechanisms for oxalate oxidase and oxalate decarboxylase, shown in Figure 1, begin with oxalate and a dioxygen molecule sequentially binding to the Mn^{2+} ion. The complex goes through a reversible proton-coupled electron transfer to yield a Mn-bound oxalate radical anion, which is decarboxylated to form CO_2 and a Mn-bound formyl radical anion. The two mechanisms then diverge. In the presence of an active site proton donor (glutamic acid), oxalate decarboxylase protonates the formyl radical anion and releases formate. Oxalate oxidase does not have an active site proton donor and it has been proposed that the formyl radical anion goes through a percarbonate intermediate, before releasing hydrogen peroxide and another mole of CO_2.

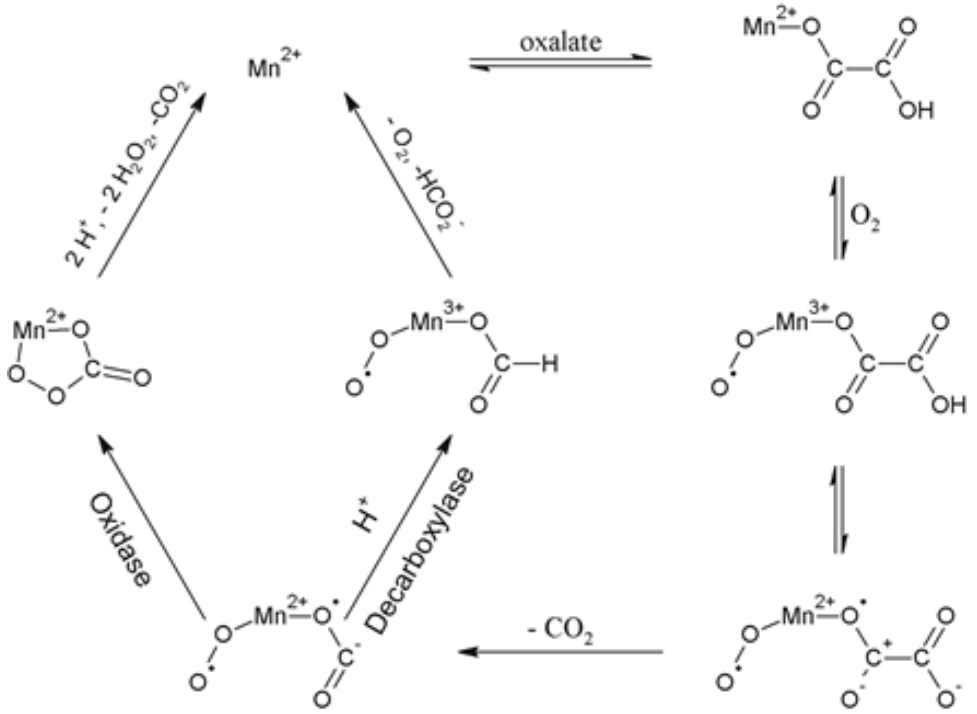

Figure 1: Model of free-radical mechanisms for oxalate oxidase and oxalate decarboxylase. Reproduced from Moussatche, *et al.*[15] which was modified from Escutia, *et al.*[16]

Oxalate Oxidase

The first fungal oxalate oxidase was reported in *Ceriporiopsis subvermispora* (CsOxOx), a white rot basidiomycete which degrades lignin.[17] When growing on wood *C. subvermispora* expresses laccase and peroxidase, which degrade the phenolic components of lignin. Peroxidase, however, requires hydrogen peroxide to degrade lignin, and CsOxOx may be involved in lignin degradation by providing hydrogen peroxide.[18] Heterologous expression of CsOxOx in *E.coli* requires the assistance of co-transformed DnaK and DnaJ chaperone proteins, but purification results only 40% pure protein.[16] CsOxOx, a soluble glycoprotein when expressed in *Pichia pastoris*, has a pH optimum of 4.0 suggesting that monoprotonated oxalate is the active form of the substrate. Site-directed mutagenesis experiments have suggested that a carboxylate residue near the active site that must be unprotonated for catalysis to occur.[19]

Kinetic parameters of CsOxOx at pH 4.0 depend on the various carboxylic acids used as buffers. Previous enzymatic characterization of CsOxOx employing a continuous spectrophotometric assay in which H_2O_2 production is coupled to the horseradish peroxidase (HRP) catalyzed oxidation of 2,2'-azinobis-(3-ethylbenzthiazoline-6-sulphonic acid) (ABTS)[20] demonstrated that the steady-state kinetic parameters of CsOxOx are sensitive to the buffer in the reaction mixture.[19] Steady-state measurements using the coupled assay carried out in acetate buffer, pH 4.0 resulted in a V_{max} value of 21.2 U/mg which compares favorably with the value obtained for the native enzyme. The K_m for oxalate, measured in acetate buffer, however, is 14.9 mM, which is significantly higher than the 0.1 mM value reported for the native enzyme. Succinate buffer, pH 4.0 yields a K_m value for oxalate of 1.5 mM while citrate buffer, pH 4.0 yields a K_m of 0.1 mM. The V_{max} in citrate is, however, reduced (V_{max} = 8.1 U/mg) and the addition of succinate increases the activity of the citrate inhibited enzyme. These results suggest that citrate may be an uncompetitive inhibitor. The addition of succinate into citrate buffer increased the activity of CsOxOx. Additionally, various carboxylic acids were found to be inhibitors of CsOxOx in previous work. Acetate, malonate, malate, pyruvate, glycolate and glyoxalate were tested as inhibitors with K_i values of 3.9 mM, 3.0 mM, 52 mM, 17 mM, 28 mM and 15 mM, respectively.[19] Uninhibited maximal reaction rates could, however, be achieved at high substrate concentrations suggesting that these molecules were competitive inhibitors. Using the HRP coupled assay, none of these molecules served as substrates.

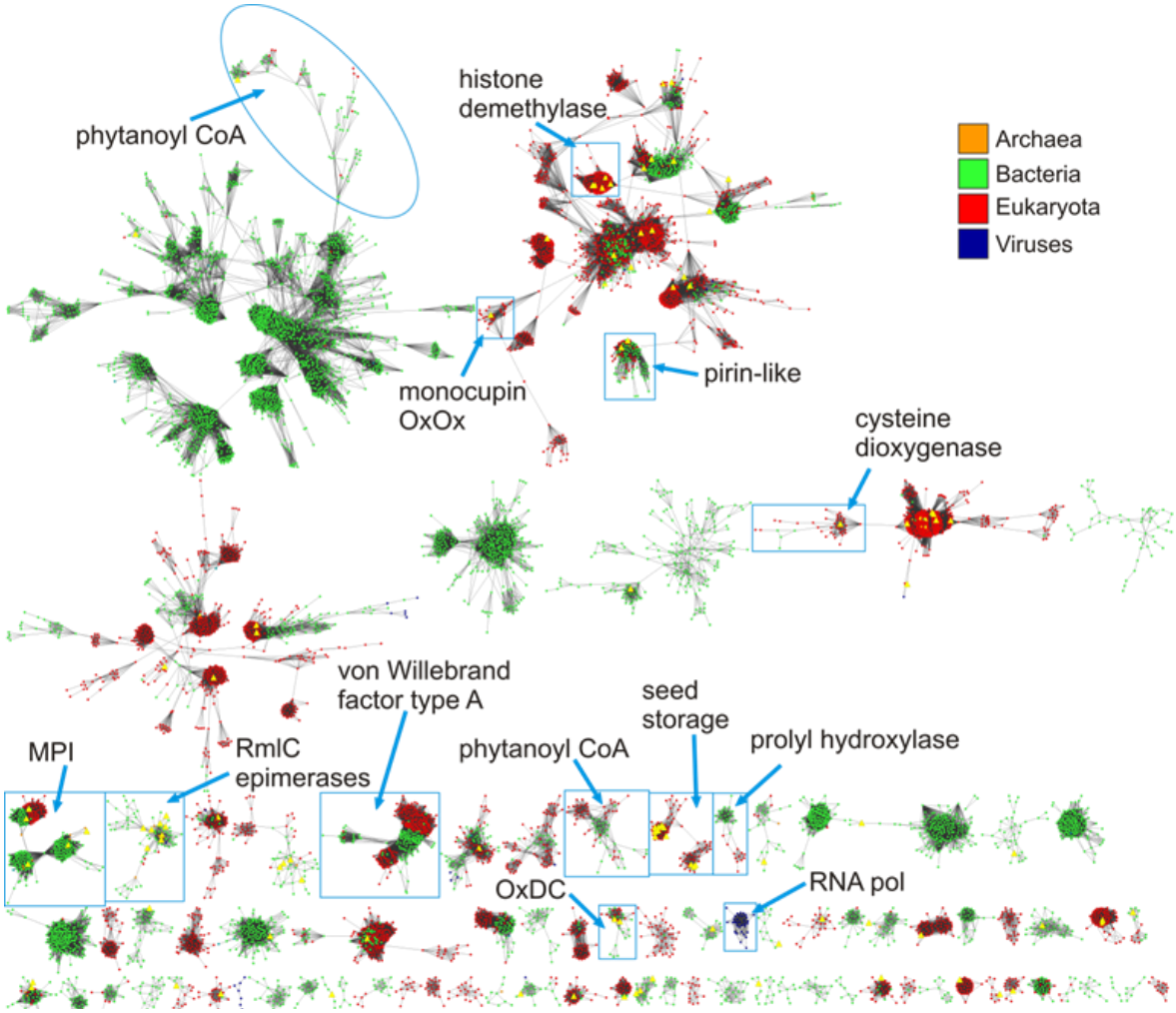

Figure 2: Representative sequence similarity network for cupin superfamily members colored by domain. Each node (14,944 representative nodes) represents a collection of sequences sharing greater that 40 % identity (252,321 unique sequences). Edges between nodes are drawn only if the E-value is less than of 1 x1026. Larger yellow nodes indicate sets of proteins in which at least one protein possesses a solved crystal structure in the PDB (Uberto *et al*, unpublished).

Mutational studies for CsOxOx have shown catalysis takes place in the N-terminal domain.[19] Mutations in the C-terminal domain, however, remove Mn in both domains suggesting both sites must be intact for Mn incorporation. These data do not preclude the C-terminal domain from carrying out catalysis. The role of the C-terminal domain in catalysis is an active area of research. CsOxOx shares 49% sequence identity of with *Bacillus subtilis* oxalate decarboxylase (BsOxDC) suggesting CsOxOx is the only oxalate oxidase that is bicupin (Figure 3). A protein

similarity network (PSN) constructed for the cupin superfamily further shows CsOxOx clustered together with other bicupin oxalate decarboxylases rather than monocupin oxalate oxidases (Figure 2) (Uberto *et al*, unpublished).

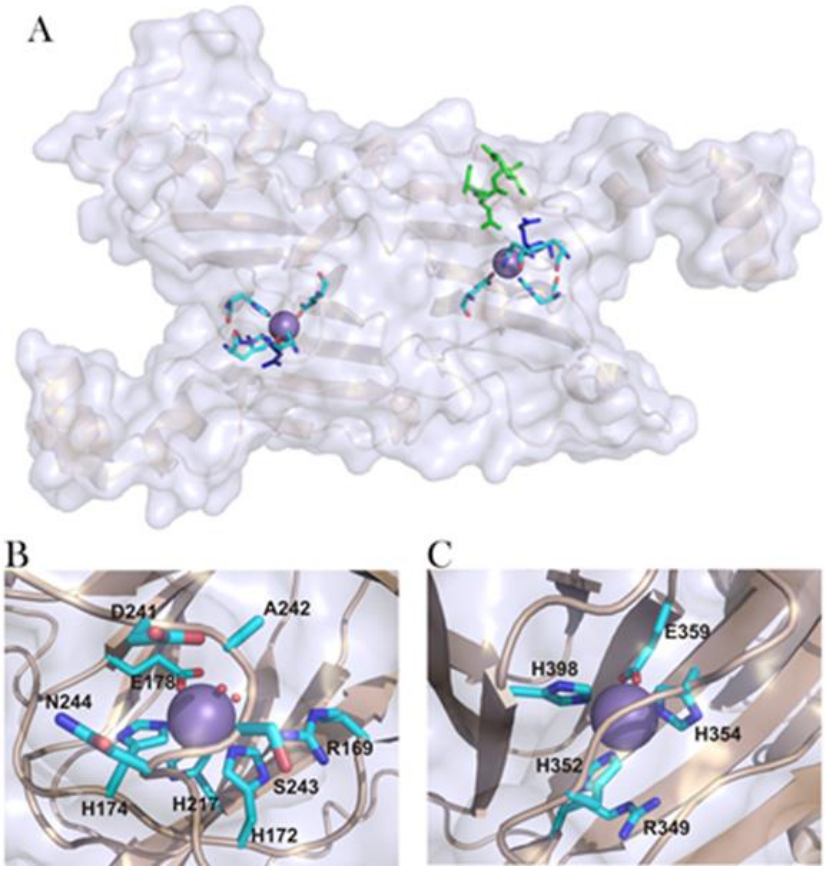

Figure 3**:** Mn binding sites of OxDC and homology models of Mn binding sites of CsOxOx. A) OxDC (PDB ID 1UW8), flexible lid region shown in green, B) N-terminal CsOxOx Mn binding site. C) C-terminal CsOxOx Mn binding site.[15]

Oxalate oxidase from *Hordeum vulgare* (HvOxOx), a germin-like protein, is a monocupin that exists as trimer of dimers, which is resistant to heat and proteases.[22] HvOxOx is strongly expressed during germination of barley embryos.[23] The active form of HvOxOx is glycosylated and contains a Mn(II) ion in the resting state. The Mn ion is coordinated by two water molecules

and four conserved residues: three histidines and one glutamate in an octahedral geometry.[24] One water molecules is removed in the presence of monodentate oxalate or both in the presence of bidentate oxalate.[25]

Recombinant expression of HvOxOx in *Pichia pastoris* yields a 140 kDa protein that is soluble in water with a specific activity of 10 U/mg.[26] Recombinant HvOxOx shows no signs of superoxide dismutase activity.[26] HvOxOx protects the plant from pathogenic fungi through the oxygen-dependent oxidation of oxalate to produce hydrogen peroxide by strengthening the cell wall of the plants; hydrogen peroxide is utilized in plant signaling as well.[27] HvOxOx is expressed in transgenic plants to protect plants from pathogenic fungi and used in detection of oxalate in the blood.[28]

Oxalate Decarboxylase

Oxalate decarboxylase is oxygen-dependent, and it cleaves the carbon-carbon bond of oxalate to produce carbon dioxide and formate. Oxalate decarboxylases are found in some plants, fungi and bacteria. Oxalate decarboxylase is utilized in plants to degrade oxalic acid created by pathogenic fungi. The bacteria *Bacillus subtilis* expresses oxalate decarboxylase (BsOxDC) in response to acid.[29] The crystal structure for BsOxDC shows the enzyme to be a bicupin with a manganese cofactor in both domains (Figure 2); the enzyme does not require organic cofactors. The biological unit of BsOxDC is 268 kDa enzyme that exists as a dimer of trimers.[30] The manganese is coordinated by four conserved residues: three histidines and one glutamic acid. EPR experiments have shown that manganese has an oxidation state of (II) in the resting state of BsOxDC.[31] BsOxDC shows an optimal activity at pH of 5.0 with an isoelectric point of 6.1.[29]

There is a controversy in the literature about which Mn-binding site of BsOxDC is the site of catalysis. One set of experiments implicated the manganese ion in the C-terminal domain to be the active site for BsOxDC. In this proposal a glutamic acid (Glu333) is proposed to protonate the formyl radical anion intermediate.[30,32] A different crystal structure of BsOxDC, however, reveals a lid region (residues 161-165) (Figure 2), which allows oxalate to diffuse into the active site and prevents bulk solvent from entering when opening and closing.[33,34] Mutational studies of the corresponding glutamic acid in the N-terminal Mn-binding site (Glu 162) and the lid region have removed decarboxylase activity and supports the hypothesis that the site of the active site is N-terminal domain. Catalysis in the C-terminal domain, however, cannot be precluded since mutations in the C-terminal domain denature the protein.[35] BsOxDC contains a small amount of oxalate oxidase activity.[36] The mutant E162Q decreases decarboxylase activity, but does not increase oxidase activity a large amount.[35] Deletion of the lid in the BsOxDC does not induce oxidase activity, but the mutations of SENS to DASN in the lid region increase oxidase activity; decarboxylase activity is returned in the mutant with the reintroduction of Glu162. [37]

Sclerotinia sclerotiorum is plant fungus that attacks and destroys important cash crops each year.[38] *S. sclerotiorum* attacks the cell walls of plants with oxalic acid and suppresses the plant's defense during an infection.[38,39] Oxalate is accumulated in the fungus, but expresses two genes to regulate the accumulation of oxalate during an infection (Ss-odc1 and Ss-odc2). Mutations in Ss-odc1 show a wild-type growth in the fungus, but mutations in Ss-odc2 disrupted appresorium development.[40] Ss-odc2 is found to have decarboxylase activity in the extract using formate dehydrogenases.

Applications of Oxalate-Degrading Enzymes

Oxalate degrading enzymes have been applied in clinical assays to test oxalate in blood and urine.[41,42] Oxalate in humans and other animals react with calcium to form calcium oxalate. Calcium oxalate makes up a large component of kidney stones.[43] Oxalate-degrading enzymes can be used to detect the onset of kidney stones in blood and urine samples.[44] Oxalate-degrading enzymes can be further utilized in the therapies of hyperoxaluria.[45]

Transgenic plants engineered to contain oxalate-degrading enzymes are used to protect plants from pathogens using oxalate to attack plants.[46,47] Multimillion dollar losses of cash crops incur each year due to attacks from pathogenic fungi.[48] These pathogenic fungi utilize oxalic acid to attack and destroy plants. Genes of oxalate-degrading enzymes are inserted into these plants. The transgenic plants then protect themselves from pathogenic fungi by expressing oxalate-degrading enzymes.[49]

The paper pulping industry employs oxalate-degrading enzymes.[50,51] Pulping is the process of transforming wood into fiber, which will be used to create paper. Enzymes are applied in bleaching in the paper pulping industry.[52] The color is bleached from the fiber by degrading lignin using traditional acids.[53] Manganese peroxidases, which utilize hydrogen peroxide, are used to degrade lignin in the bleaching process.[54] Oxalate oxidase produces hydrogen peroxide as a product, which is utilized by peroxidases. Oxalate-degrading enzymes reduce the environmental and manufacturing costs in the paper pulping industry by replacing harsh chemicals with enzymes and maintain fiber integrity.

There is active research for the application of oxalate-degrading enzymes for use in biofuel cells.[55-57] Biofuel cells differ from traditional battery cells in that biofuel cells commonly utilize oxidoreductases as an electrocatalysts to oxidize biomass.[58] The electrons released from the oxidation are then transferred to an anode. The current supplies the cathode with electrons, which are used in the reduction of organic compounds by reductases.[58,59] A membrane separates the oxidases and reductases and forces the electrons to flow through a circuit. Biofuel cells are more desirable since they are friendlier on the environment and bypass thermodynamic limitations of combustion by electrochemical conversion. Biofuel cells face challenges to become an efficient source of energy. One major problem is the direct electron transfers from the enzyme to the electrodes. Enzymes can immobilized onto the surface of the anode to facilitate better electron transfer, but immobilizing enzymes onto the surface of the electrodes can result in reducing or abolishing the activity of the enzyme.[60] One solution is the use of mediators to transfer electrons released from the enzyme to the electrodes.

There are two types of electron transfers used in electrochemical systems: mediated electron transfers (MET) and direct electron transfer (DET). Mediated electron transfer uses small molecules to mediate the transfer of electrons between the enzymes and electrode. The maximum voltage of a biofuel cell is constrained by the thermodynamic redox potentials of the mediators. Electrons transfer from the enzyme to the electrode in direct electron transfer.[58] The rate of electron transfer in DET is improved when the distance between the donor and acceptor is the shortest.[61] Enzyme immobilization is utilized in DET, but faces obstacles in maintaining its

activity. Engineering enzymes can overcome difficulties associated with creating an efficient biofuel cells.[62]

Oxalate-degrading enzymes have been shown to be utilized as an electrocatalysts in biofuel cells. Oxalate oxidase or oxalate decarboxylase is combined with 4-amino TEMPO (2,2,6,6-tetramethylpiperiidine-1-yl)oxyl) to oxidize glycerol to CO_2, which releases 16 electrons per molecule.[63,64] TEMPO performs the first five steps of oxidation of glycerol to mesoxalate (glycerol $\rightarrow$ glyceraldehyde $\rightarrow$ glyceric acid $\rightarrow$ 2-hydroxy-3-oxopropanoic acid $\rightarrow$ tartronic acid $\rightarrow$ mesoxalate). OxOx or OxDC converts mesoxalate to glyoxalic acid. Glyoxalic acid is then oxidized by TEMPO to produce oxalate, which is then completely oxidized by OxOx or OxDC. The small pH overlap of OxOx and OxDC and TEMPO and the conversion of mesoxalate to glyoxalic acid limit the rate of the cascade. Engineering the enzymes to increase the overlap of pH with TEMPO will allow a better rate for the cascade. The starting fuels able to be utilized can be increased by engineering the enzymes with wider substrate specificities. Biofuel cells using oxalate degrading enzymes can be further optimized by engineering rates for the reaction using mesoxalate.[65]

Enzyme promiscuity

There are two types of enzymes promiscuity: substrate (substrate ambiguity) and catalytic promiscuity (reactions proceeds through different transitions states with different substrates).[66,67] Numerous of reports of enzyme promiscuity in the last 20 years has led some researchers to believe that very few enzymes have high selectivity for a single molecule, and that most have

activity for other substrates, albeit in low activity. For instance, many enzymes in the amidohydrolase superfamily are promiscuous with other substrates that correspond to functions of other members within the same family.[68] Moreover, many toxin-degrading enzymes are promiscuous since they encounter numerous and unfamiliar molecules.[69]

There are several reasons why promiscuity exists in enzymes. Promiscuity may exist because exact substrate specificity is impossible, since molecules that are small enough to fit into the active site may be positioned in multiple orientations resulting in variable reactivities of amino acids in close proximity.[66] Another reason is that enzyme promiscuity is a relic of ancestral enzymes which had general specificity. Through mutations, however, enzymes obtained higher specificity for molecules while retaining the ancestral fold that enabled additional reactions or substrate preferences. Through duplication and divergence of genes, these enzymes gave rise to superfamilies with additional catalytic mechanisms and substrate specificity.[70,71] A repertoire of chemical reactions allows for enzyme evolution in the presence of constant selective pressures. Enzymes that are too specific cannot improve in their fitness, but promiscuous enzymes can improve fitness through mutations. Directed evolution can be applied to promiscuous enzymes to improve activity, where they are used in various aspects of biotechnology.[72]

Conformational changes to the active site of enzymes enable binding to alternative substrates.[73] Substrates small enough to fit inside the active site may form non-covalent interactions with the enzymes.[73] Promiscuity may favor hydrophobic interaction in contrast to electrostatic interactions, since electrostatic forces are dependent on the orientation of the functional groups.[74] Post-translational modifications and cofactors can influence the promiscuity of enzymes. The

promiscuity of two phosphonate monoester hydrolases from *Pseudomonas aeruginosa arylsulfatase* and *Rhizobium leguminosarum* emerges from the modification of the cysteine residue in the active sites to formylglycine.[75] Like oxalate degrading enzymes, a large percentage of promiscuous enzymes have metal cofactors. For example, most enzymes in the alkaline phosphatase superfamily are promiscuous, which mostly contain zinc as their cofactor.[76]

Isothermal Titration Calorimetry

Direct measurement of enzymatic reaction rates has numerous advantages over a coupled assay. Previously, the Moomaw Laboratory reported use of membrane inlet mass spectrometry (MIMS) as a direct and continuous method to measure oxalate oxidase activity.[21] In the MIMS assay method, doubly labeled ^{13}C oxalate is used in order to distinguish the CO_2 generated by CsOxOx from adventitious CO_2 dissolved in the reaction mixtures. Since the use of labeled substrates places constraints of expense and availability on the molecules tested for activity as substrates, we investigated the applicability of the multiple injection method of isothermal titration calorimetry for the direct detection of the CsOxOx catalyzed oxidation of oxalate.

Chemical reactions (both enzymatic and non-enzymatic) consume (endothermic) or release (exothermic) heat. There are various calorimetric methods used to measure the heat changes produced during reactions. Isothermal titration calorimetry (ITC) is used to measure binding and kinetic parameters.[77] ITC, a thermal compensation instrument, measures the differences in temperature between two cells: a sample and reference cell. Shown in Figure 4, the sample-containing syringe (titrant) inserted into the buret handle automatically injects a programmed

amount of titrant into the enzyme-containing sample cell. The heat produced or consumed is measured by sensitive sensors surrounding the sample and reference cells. The differences in temperature between the sample and reference cells are compensated for by an increase or decrease in thermal power applied onto the sample cell. The thermal power (work) that is required to maintain isothermal conditions is monitored.

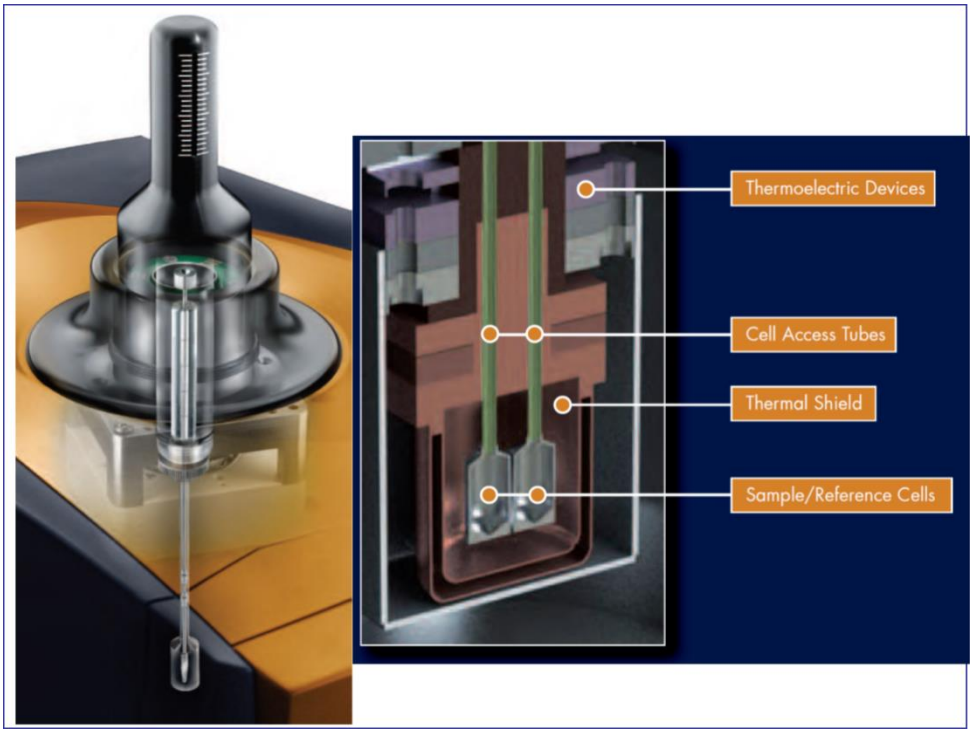

Figure 4: Schematic diagram of the TA Instruments ITC.

There are protocols by which the ITC can be used to determine the kinetic parameters of enzyme catalyzed reactions: the multiple injection method and the single injection method.[78] The multiple injection method is a series of injections separated by 2-4 minute time intervals. The enzyme concentration in the sample cell is smaller than the substrate concentration contained in the syringe, which is greater than its K_m. The baseline, after each injection, is used to calculate

the rate upon each injection. The single injection method is a single injection of substrate contained in the syringe into the enzyme-containing sample cell over an hour. Thermal power is monitored continuously as the substrate is converted to product, and it returns to baseline as all substrate is consumed. The continuous thermal power required to maintain isothermal conditions is converted to rate. The rate plot for the single injection is continuous whereas that of the multiple injection method is discrete.

Isothermal titration calorimetry can extract thermodynamic and kinetic parameters for enzymes. It can also be used to test potential substrates possibly allowing for medium-to-high throughput screening of substrates even when the products formed are not known. Activation energy of enzymes can be determined using isothermal titration calorimetry experiments measuring reaction rates at a range of temperatures. Extraction of enthalpy and entropy of activation can be achieved by creating an Eyring plot.[79] Kinetic parameters from the Eyring plot are determined at each temperature, and the natural logarithm of each k_{cat} divided by temperature ($\ln(k_{cat}/T)$) is plotted against its corresponding temperature in kelvin (1/T). A linear regression is performed on the data points to obtain a linear curve. The enthalpy of activation is obtained from the slope of the curve, and the entropy of activation is obtained from the y-intercept of the curve.[79]

Alternatively, energy of activation (E_a) can be extracted from the slope of the Arrhenius plot, which can also derive enthalpy and entropy of activation at specific temperature. The ln(k) is plotted against the reciprocal absolute temperature (1/T) instead of plotting the $\ln(k_{cat}/T)$ against the reciprocal absolute temperature (1/T).[80] The E_a is obtained through the slope of the regression fit. An Arrhenius plot of the oxalate oxidase activity of BsOxDC is shown in Figure 5. The

thermodynamic parameters are obtained through the relationship between E_a and the enthalpy of activation, which allows the extraction the entropy and Gibbs free energy of activation. The data in Figure 5 provide an estimate of 7.8 ± 0.4 kcal/mol for the overall activation energy of the oxidation activity of BsOxOx. An Arrhenius plot of mutant variants of the enzymes can be superimposed onto the wild-type enzyme to determine the thermodynamic basis of the change in reaction.[79] Coupled with site-directed mutagenesis, the Arrhenius plot can be used to guide protein engineering of enzymes to optimize a reaction by observing the thermodynamic changes in the mutants.[81]

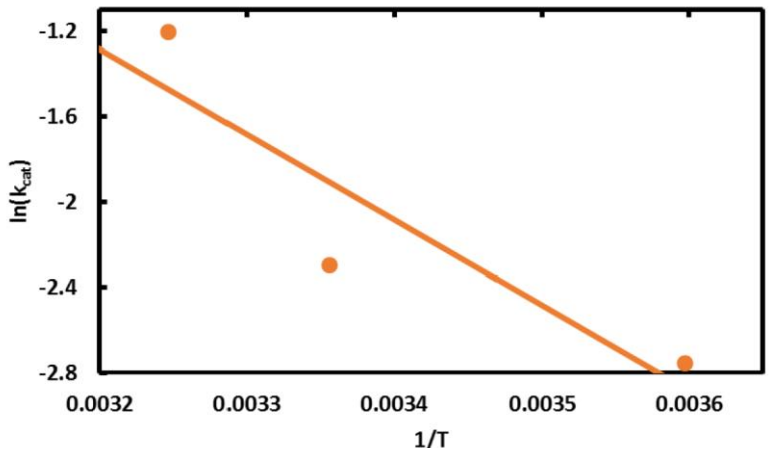

Figure 5: Arrhenius plot of lnk_{cat} against the reciprocal of absolute temperature. Reproduced from Molina, *et al*.[82]

Circular Dichroism

Secondary protein structure can be monitored by circular dichroism (CD) and therefore, the effects of temperature on secondary structure can be reported on. Unlike X-ray crystallography,

CD cannot sufficiently characterize protein structure by elucidating the position of all the atoms in the protein. CD, however, can give a composite spectrum for a sample representing the overall secondary structural elements.[83]

CD works by polarizing light into two forms: left-handed and right-handed polarized light. The resultant vector formed by superimposing the two forms is linear.[84] As the two forms pass through the cuvette containing the protein solution, right and left polarized light are absorbed differently by the sample. The two forms of light with different magnitudes are superimposed to give a resultant vector that is elliptical, which is measured against the wavelength.[83]

Ellipticity arises only when the molecule of interest is chiral, as left-handed and right-handed polarized light are only absorbed by chiral molecule. Since all natural amino acids are chiral, except glycine, the overall secondary protein structure is chiral. The secondary structure of proteins is measured in the far UV (220-185nm), whereas tertiary structure is measured in the near UV (260-310nm) where tryptophan, tyrosine and phenylalanine absorb. One major application of CD is to investigate thermal denaturation of proteins by measuring the degree of ellipticity at a specific wavelength against temperature.[85] By fitting various equations onto the melting curve, the Tm, the temperature at which half of the molecules are denatured, values of ΔH, ΔS and ΔG are extracted. [83,86]

ITC is a powerful instrument to unveil chemical reactions without any chemical or physical modifications to the enzymes or substrates. Previous study has shown that small carboxylic acids

were inhibitors of CsOxOx at low concentrations of substrate.[19] The study, however, does not preclude the possibility that the inhibitors are potential substrates. The use of spectrophotometric assays is difficult because often the products of enzymatic reactions are spectrophotometrically silent. This situation may be overcome by chemical modifications to the enzyme or by coupling the product of reaction to another enzyme. ITC can alleviate this obstacle by measuring the thermal power required to maintain isothermal conditions after the heat released from a chemical reactions. Thus, ITC can be used to assess whether or not the small carboxylic acids previously shown to be inhibitors serve as alternative substrates.

The long term goal in the Moomaw laboratory is to understand how protein structure modulates catalytic function. One overarching question is how do evolutionary-related proteins that are structurally similar carry out different reactions using the same substrate? The studies described in the following work are designed to characterize the thermal and kinetic parameters of the CsOxOx catalyzed reactions in order to lay the ground work for a comparison of these results with evolutionary-related proteins. It is anticipated that the application of ITC to the study of oxalate degrading enzymes will provide insights into their evolutionary history and to their development for use in biofuel cells.

CHAPTER 2. METHODS AND MATERIALS

Unless otherwise stated, all chemicals and reagents were purchased from Sigma-Aldrich and were of the highest available purity. The concentration for CsOxOx was determined using the Lowry method standardized with bovine serum albumin.[87]

Expression and Purification of CsOxOx

Recombinant oxalate oxidase from *Ceriporiopsis subvermispora* was expressed and purified as a secreted soluble protein using a *Pichia pastoris* expression system as previously described.[19] The gene of the G isoform of CsOxOx was amplified using PCR. Xbal and Xhol restriction enzymes were used to digest the PCR product, which contained an Xbal restriction site at the 5' end and an Xhol at the 3' end. This fragment was ligated into Xbal and Xhol digested pPICZαA vector. The cloned vector was used to transform *Pichia pastoris* X-33 strain using Invitrogen's EasyComp transformation kit. Colonies were screened for Zeocin resistance as well as the ability to grow in media with methanol as the sole carbon source of energy.

The successfully screened colonies of recombinant CsOxOx were used to inoculate twenty-five milliliters of MGY media in a 250 mL baffled flask, which contained 1.34% yeast nitrogen base, 1% glycerol, 4X10-5 % biotin. The flasks were grown overnight shaking at 250 rpm at 28-30 ^{o}C until the log phase growth (OD_{600}= 2-6) had been reached. The cells were resuspended in 500 mL of MM media to induce the expression of CsOxOx after harvesting the cells through

centrifugation at 2500 x g for five minutes. Every 24 h for 4-5 days, methanol was added to resuspended cells, which were grown 28-30 ^{o}C with shaking at 250 rpm. The cells were harvested through 5000 x g centrifugation at 15 ^{o}C for 45 minutes, the media that contained the secreted CsOxOx was concentrated using Millipore's stirred cell ultrafiltration and Biomax-30 tangential flow cassette. The concentrated CsOxOx was applied to a DEAE-Sepharose Fast Flow column after being extensively dialyzed against 50 mM Imidazole-Cl (pH 7.0). 50 mM Imidazole-Cl (buffer A) was used to equilibrate the column. The protein was eluted by a linear gradient from buffer A to the same buffer with NaCl. Fractions of oxalate oxidase activity were pooled, and solid $(NH_4)_2SO_4$ was added to the sample to 1.7 M. The CsOxOx was purified further by applying the solution to a butyl-Sepharose column and eluting the protein with a linear gradient from buffer B (50 mM Imidazole-Cl containing $(NH_4)_2SO_4$) to buffer A. The fractions were pooled, concentrated and dialyzed against 25mM Imidazole-Cl (pH 7.0).

Continuous Spectrophotometric Assay of CsOxOx

A continuous spectrophotometric assay was used to measure steady state kinetics of CsOxOx. The H_2O_2 produced from the reaction was coupled to horseradish peroxidase, which catalyzes the oxidation of 2,2'-azinobis-(3-ethylbenzthiazoline-6-sulfonic acid) (ABTS). The reaction solutions contained 50 mM potassium oxalate, 5 mM ABTS, 25 U horseradish peroxidase and CsOxOx dissolved in solution containing 50 mM sodium succinate (pH 4.0). The assay measured the activity of CsOxOx at wavelength of 650 nm. The extinction coefficient for ABTS was assumed to be 10,000 M^{-1} cm^{-1}. CsOxOx was omitted in the controls samples to observe any oxygen-dependent dye oxidation by horseradish peroxidase.

Isothermal Titration Calorimetry

All ITC experiments were carried out using a two-cell (sample cell and reference cell), low-volume Nano ITC (TA Instruments, Inc.). All samples used in the ITC were degassed. A 50μL stirred injection syringe inserted into the burette handle was used to inject substrate or enzyme into the 24 K gold, 190 μL volume sample cell. Water was used in the reference cell for all ITC experiments. Heat (Q) produced during catalysis was measured by the continuous supply of instrumental thermal power (dQ/dt) to the sample cell, which maintains isothermal condition between the sample cell and reference cell. Thermal power relates to enzyme reaction rate:

$$\frac{dQ}{dt} = \frac{d[P]}{dt} \times V \times \Delta H_{app}, \quad [1]$$

where V is the volume of the solution in the sample cell, ΔH is the apparent enthalpy and (d[P])/dt is the enzyme reaction rate. When equation [1] is solved for (d[P])/dt, the resulting equation is:

$$\frac{d[P]}{dt} = \frac{1}{V \times \Delta H} \times \frac{dQ}{dt}. \quad [2]$$

Using Nano Analyze (TA Instruments, Inc.), raw ITC data was transformed into rate data using the equations above, which was fitted against the Michaelis-Menten equation to obtain the kinetic parameters for oxalate and mesoxalate.

Multiple Injection Method

The multiple injection ITC method of measuring OxOx activity involves continuous, real-time detection of the amount of heat generated (dQ) during catalysis, which is equal to the number of moles of product produced times the enthalpy of the reaction (ΔH_{app}). Determination of the kinetic parameters of a reaction using this method, therefore, requires two experiments 1) determination of the enthalpy of the reaction from the complete conversion of substrate to product, and 2) determination of the differential power effects from the continuous conversion of substrate to product.

The complete conversion substrate to product requires the concentration of enzyme to be significantly higher than the concentration used in the determination of the kinetics. The concentration of substrate is less than the K_m to ensure the complete conversion of substrate to product as the substrate is injected into buffer solution containing the enzyme. The injection of substrate into buffer solution containing the enzyme produces a peak as a result of the heat produced from the reaction, which returns to pre-injection baseline as the substrate is converted to product. The enthalpy is obtained from equation [3] by taking the area under the peaks and dividing the area by the moles of product.

$$\Delta H_{app} = \frac{1}{[S]*V} \int_{t=0}^{t=\infty} \frac{dQ}{dt} dt \quad [3]$$

The kinetic experiment of the multiple injection method requires the substrate concentration in the syringe to be higher than the K_m of the enzyme. The low concentration of enzyme is used to allow the continuous turnover of substrate to product, which is exhibited by a shift in the baseline. The baseline is averaged over a time to obtain the average thermal power shift, which is used in equation [2] to determine the rate of product formation. The rate of product formation is plotted against the substrate concentration for each injection. A non-linear regression of Michaelis-Menten equation was fitted onto the plot, and kinetic parameters were extracted.

Arrhenius Plot

All of the experiments for the Arrhenius plot were performed with Nano ITC (TA Instruments, Inc.) 500 nM CsOxOx in 50 mM succinate buffer, pH 4.0. The enzyme was incubated in the sample prior to the run for thirty minutes at each temperature. The Arrhenius plot was obtained from measuring kinetic parameters for CsOxOx at a range from 20 to 45 ^{o}C with 5 ^{o}C intervals. The apparent enthalpy was obtained for each temperature. The ln(k_{cat}) is plotted against the reciprocal of the absolute temperatures. The thermodynamic parameters are obtained from the linear fit of equation [4] onto the plot. The E_a was obtained by multiplying the slope by – R.

$$\ln K_{cat} = \frac{-E_a}{T} + \ln(a) \quad [4]$$

$$\Delta H^{\ddagger} = E_a - RT \quad [5]$$

The thermodynamic parameters were obtained at specific temperatures. The relationship between E_a and ΔH used in equation [5] obtains the enthalpy of activation. The Gibbs free energy of activation was obtained from equation [6] using the kinetic parameters for the specific temperature. The entropy of activation was obtained from equation [7] using the enthalpy and Gibbs free energy of activation obtained from the previous equations.

$$\Delta G^{\ddagger} = RT(23.76 + \ln T - \ln K_{cat}) \text{ [6]}$$

$$\Delta S^{\ddagger} = \frac{\Delta H^{\ddagger}}{T} - \frac{G^{\ddagger}}{T} \text{[7]}$$

Circular Dichroism

All Circular Dichroism (CD) experiments were performed using a JASCO J-1500 Spectropolarimeter (JASCO Inc., Tokyo, Japan) using a 0.1-cm path length cell. All samples were exchanged into 25 mM potassium phosphate (pH7.0). Analysis of CD spectra was performed using Spectra Analysis (JASCO Inc., Tokyo, Japan).

Serially diluted CsOxOx samples at 3.0, 1.5, 1.0, 0.7, 0.5 and 0.33 mg/mL were recorded at wavelengths over the range of 195-250 nm. The scan rate and bandwidth were 10 nm/min and 1

nm, respectively. Each spectrum was an accumulation of five scans. A blank spectrum was performed with buffer and subtracted from the spectra.

In order to observe the effects of thermal denaturation on the secondary structural elements of CsOxOx, spectra were recorded of a 0.68 mg/mL sample in 25 mM potassium phosphate buffer, pH 7.0 at increasing temperatures (10 ^{o}C to 90 ^{o}C, with 10 ^{o}C increments). Each spectrum was taken after ten minutes of incubation at each temperature. A Teflon stopper was used to retard evaporation. The scan rate, time constant and numbers of scans were 10 nm/min, 2 s, and 3, respectively.

A melting curve experiment was carried out to determine the melting temperature and the thermodynamic parameters for unfolding. The change in ellipticity was monitored as a function of temperature at a specific wavelength of 218 nm using 1.5 mg/ml sample of wild-type CsOxOx in 25 mM potassium phosphate (pH 7.0). Measurements were collected at intervals of 1 ^{o}C with ramping temperatures ranging from 0 ^{o}C to 110 ^{o}C. The ramping temperature ranged from 0 ^{o}C to 110 ^{o}C with intervals of 1 ^{o}C. A reverse scan (110 ^{o}C to 0 ^{o}C) was performed shortly afterwards to determine the reversibility of unfolding.

CHAPTER 3. RESULTS AND DISCUSSION

Isothermal titration Calorimetry

Direct measurement of enzymatic reaction rates has numerous advantages over a coupled assay. Previously, the use of membrane inlet mass spectrometry (MIMS) was reported as a direct and continuous method to measure oxalate oxidase activity.[21] In the MIMS assay method of CsOxOx doubly ^{13}C labeled oxalate is used in order to distinguish the CO_2 generated by CsOxOx from adventitious CO_2 dissolved in the reaction mixtures. Since the use of labeled substrates places constraints of expense and availability on the molecules tested for activity as substrates, we investigated the applicability of the multiple injection method of isothermal titration calorimetry for the direct detection of the CsOxOx catalyzed oxidation of oxalate.[20]

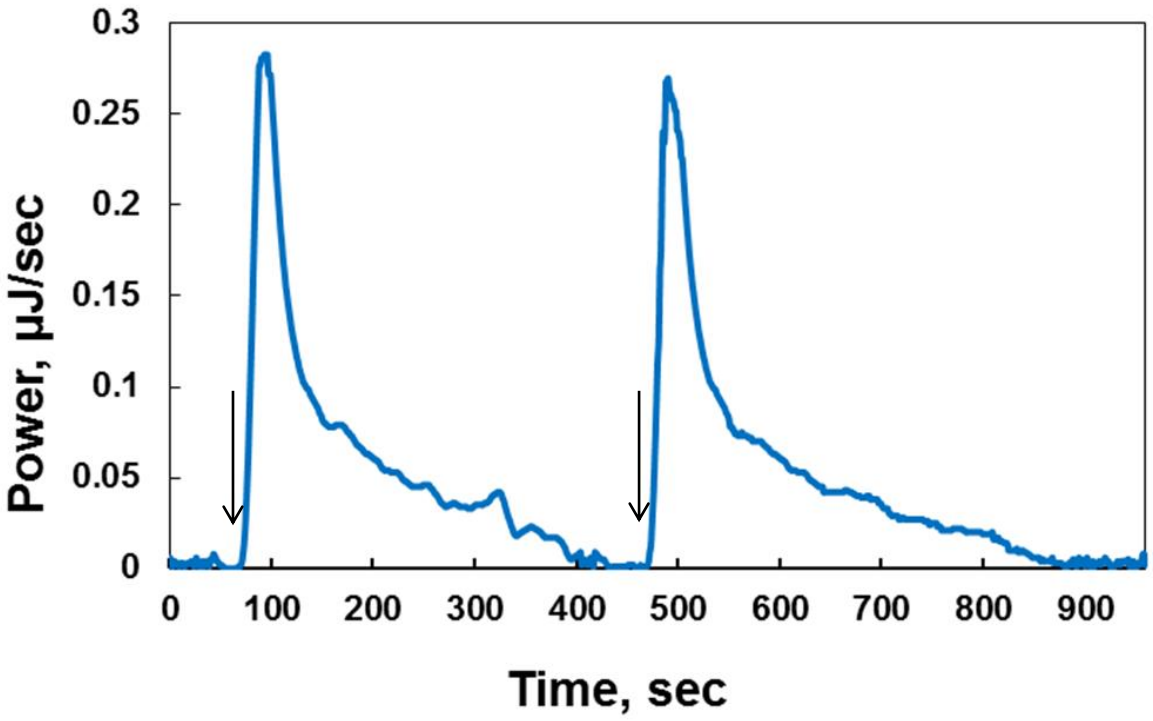

Figure 6: CsOxOx catalyzed complete conversion of oxalate into products gives the ΔH_{app} of reaction. After equilibration at 25 °C (not shown), the reaction was initiated by the addition of 1 µL of 2 mM potassium oxalate, pH 4.0 into 500 nM CsOxOx (200 µL) in 50 mM sodium succinate, pH 4.0 (first arrow). This was repeated (second arrow) again.

Succinate buffer, pH 4.0, was selected for these studies in an effort to maximize the k_{cat} and minimize the K_m. Using these conditions, the apparent enthalpy of the CsOxOx reaction was determined by measuring the amount of heat produced during the complete conversion of substrate into product. A typical calorimetric trace (heat flow as a function of time) is shown in Figure 6. The 200 µL reaction contained 500 nM CsOxOx was allowed to reach thermal equilibrium at 25 °C prior to the experiment. The baseline was collected for 1 minute then the experiment was initiated by the addition of oxalate (prepared in the enzyme dialysate) to a final concentration of 0.010 mM. The response time of the instrument can be observed to be about 18 seconds after which the heat produced by the enzyme was registered as thermal power necessary to maintain isothermal conditions. The direction of the baseline was positive for the exothermic

reaction. After the complete consumption of the substrate, the power returned to the original baseline. Four hundred seconds after the first injection, a second identical injection was made into the same reaction mixture (now containing product) resulting in a calorimetric trace almost identical in area and shape indicating that product inhibition was negligible. A blank titration of oxalate into buffer was collected (data not shown) and that heat was subtracted from that of the substrate into enzyme titration resulting in an experimental ΔH_{app} value of -5.6 ± 0.3 kJ/mol.

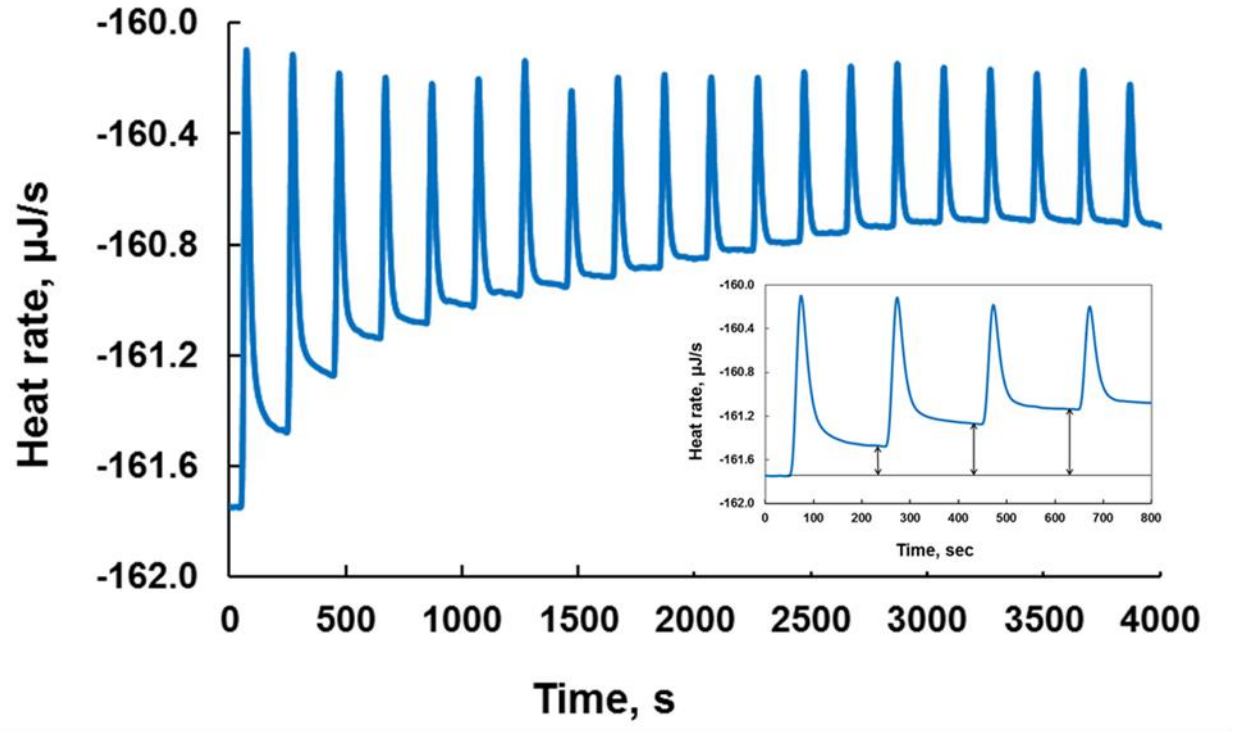

Figure 7: Thermogram monitoring the power required to maintain isothermal conditions of 20 successive injections of 2 µL of 20 mM oxalate into 112 nM oxalate oxidase (200 µL) previously thermally equilibrated at 25 ^{o}C. Under these conditions, when the enzyme velocity reaches a new steady state, the power remains constant. The inset corresponds to the first four injections of substrate into the sample cell and the arrows represent the decrease in the heat flow (dQ/dt) required to maintain thermal equilibrium at each steady state condition.

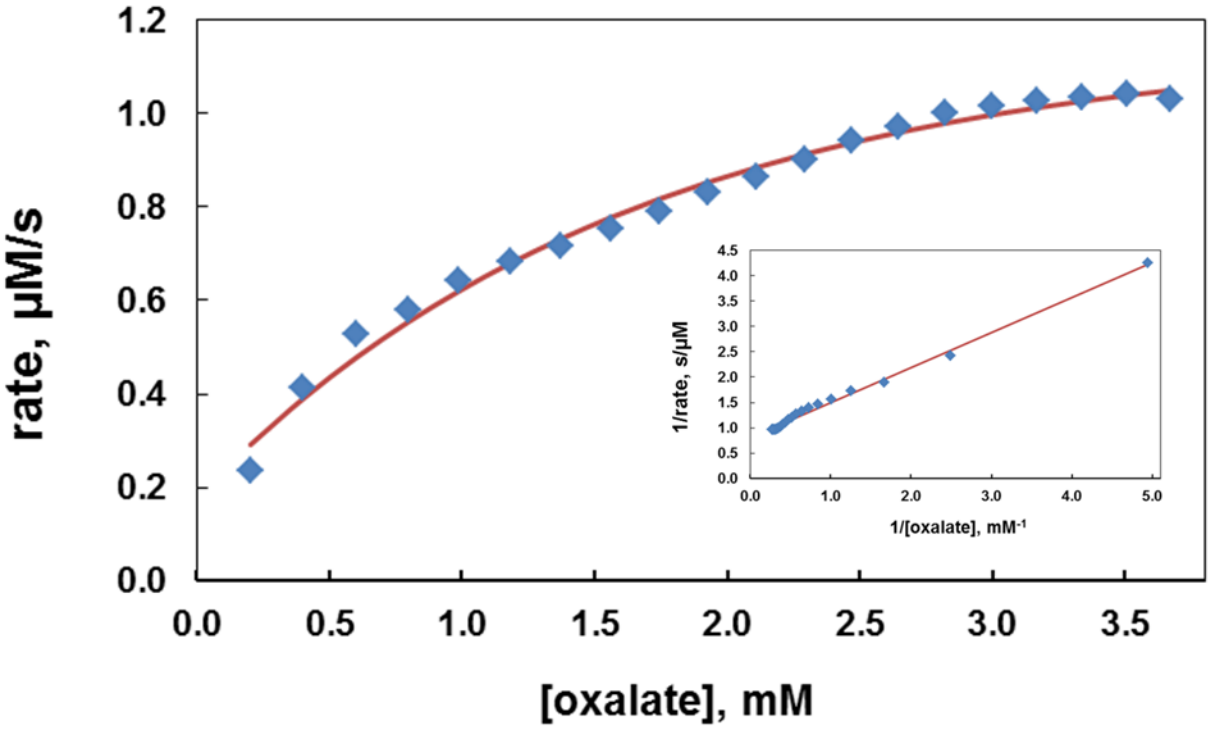

Figure 8: Rate versus oxalate concentration data from Figure 7 fitted to the Michaelis-Menton equation to give kinetic parameters provided in Table 1. The inset shows the same data in a double reciprocal plot which yielding the nearly identical values of k_{cat} and K_m as the fit to the Michaelis-Menton equation.

The differential power effects from the continuous conversion of oxalate to carbon dioxide and hydrogen peroxide is shown in Figure 7. After thermal equilibration, injections of oxalate were made every 200 seconds into a solution originally 114 nM CsOxOx resulting in final oxalate concentrations ranging from 0.200 mM to 3.700 mM (due to volume increase). The rate of the uncatalyzed reaction is negligible and the plateaus reached between injections indicate that at each new concentration of substrate a new constant [ES] is achieved. The inset in Figure 7 shows the first four injections of oxalate into the sample cell, and the arrows represent the decrease in the instrumental power required to maintain isothermal conditions at each injections (dQ_1/dt, dQ_2/dt, and dQ_3/t). The Michaelis-Menten equation was used to fit these data (Figure 8). The inset in Figure 8 displays the same data in a Lineweaver-Burk plot. The kinetic parameters are

shown in Table 1 along with those determined by the membrane inlet mass spectrometry assay and the horse radish peroxidase coupled assay.[19,21] There is good agreement among the three methods.

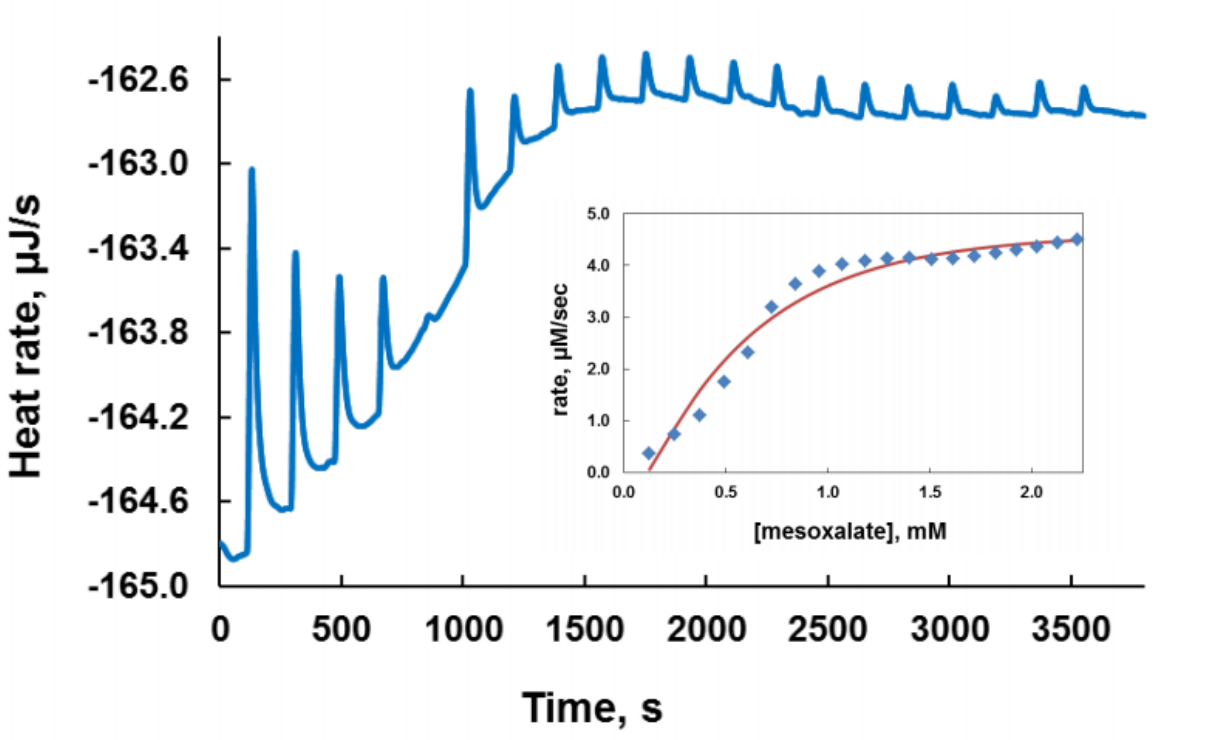

Figure 9: The heat flow as a function of time for the reaction catalyzed by CsOxOx using mesoxalate as substrate measured in conditions of steady-state kinetics at 25 ^{o}C. The sample cell contained 200 µL of 456 nM CsOxOx and 20 injections of 2.5 µL of 10 mM mesoxalate were performed with an interval of 180 seconds separating between them. The inset shows the Michaelis-Menten fit of the data, which was obtained from the conversion of heat rate. The ΔH_{app} of reaction used in the conversion was experimentally determined to be -3.1 kJ/mol (data not shown).

Mesoxalate is a substrate for CsOxOx with kinetic parameters comparable to those of oxalate. Given the interest in oxalate oxidase as a component of enzymatic biofuel cells, the ability of CsOxOx to catalyze a reaction was tested using mesoxalate (oxopropanedioic acid) as the substrate.[55,57] A typical heat flow versus time plot for the reaction catalyzed by CsOxOx using mesoxalate as substrate under steady-state kinetics is shown in Figure 9. In the experiment shown the sample cell contained 200 µL of 456 nM CsOxOx and 20 injections of 2.5 µL of 10 mM mesoxalate (final concentrations ranged from 0.125 to 2.224 mM) were performed with an interval of 180 seconds between them. The inset shows the Michalis-Menten plot of mesoxalate after converting the average thermal power of the baseline for each injection into rate. Although the shape of the data was not an ideal rectangular hyperbola, the steady state data was fit to the Michaelis-Menton equation and corrected for the enthalpy of reaction. The K_m= 0.52 ± 0.03 mM for the reaction using mesoxalate which is slightly lower that for the reaction using oxalate. The k_{cat}= 9.9 ± 0.3 s^{-1} which is two thirds of the rate using oxalate as determined by ITC (Table 1).

The ABTS dye oxidation assay results in a 20 fold lower k_{cat} value (0.5 s^{-1}) and a K_m value of 29 mM (data not shown). The predominant products of CsOxOx catalyzed reaction of mesoxalate are proposed to be glyoxalic acid and carbon dioxide making this reaction invisible in the ABTS assay. Membrane inlet mass spectrometry was used to detect carbon dioxide formation (data not shown) but was unable to quantify the rate without ^{13}C labeled mesoxalate which is currently prohibitively expensive. One possible reason why a secreted enzyme of a white rot fungus would use mesoxalate as a substrate is that the common reed (*Phragmites australis*) secretes gallic acid which is photodegraded into mesoxalate in order to ward off encroaching plants. [88]

Table 1: Steady-state kinetic parameters for the CsOxOx catalyzed oxidation of oxalate measured by ITC, membrane inlet mass spectrometry and the horse radish peroxidase coupled assay.

Assay	K_m (oxalate), mM	k_{cat}, s^{-1}	k_{cat}/K_m, $mM^{-1}\,s^{-1}$
ITC	0.86 ± 0.1	15.6 ± 0.3	18.0 ± 0.3
MIMS	0.93 ± 0.1	22.3 ± 0.3	24.0 ± 0.4
ABTS	1.5 ± 0.1	20.0 ± 0.4	13.3 ± 0.4

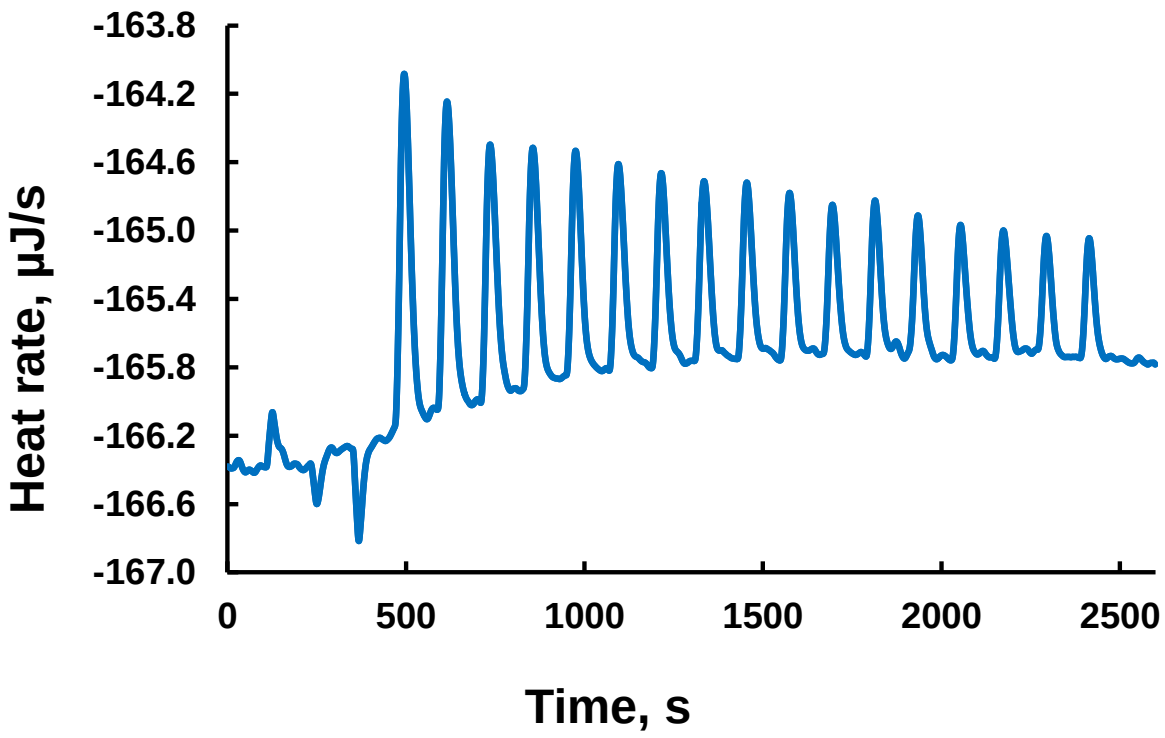

Figure 10: Calorimetric assay of oxalate oxidase using malonate as the substrate. 500 nM of oxalate oxidase (180 µL) in 25 mM sodium succinate (pH 4.0) was equilibrated at 25 °C. After 100 seconds, 2.5 µL of 100 mM malonate, pH 4.0 was injected every 120 seconds for 20 injections followed by a final 100 second period of data collection. The power required to maintain isothermal conditions is shown. Nanoanalyze (TA Instruments) was used to determine the kinetic parameters as described in the Materials and Methods section using an enthalpy value of -2.8 kJ/.mol (data not shown)

ITC results of mesoxalate prompted us to reevaluate molecules that appeared as competitive inhibitors in the spectrophotometric ABTS assay as substrates whose products are

spectroscopically silent. Glyoxalate, malonate and pyruvate have shown to be substrates using ITC to measure activity (Figure 10, 11 &12). Malate does not serve as a substrate (data not shown). The activity for the alternative substrates is lower than oxalate shown in Table 2.

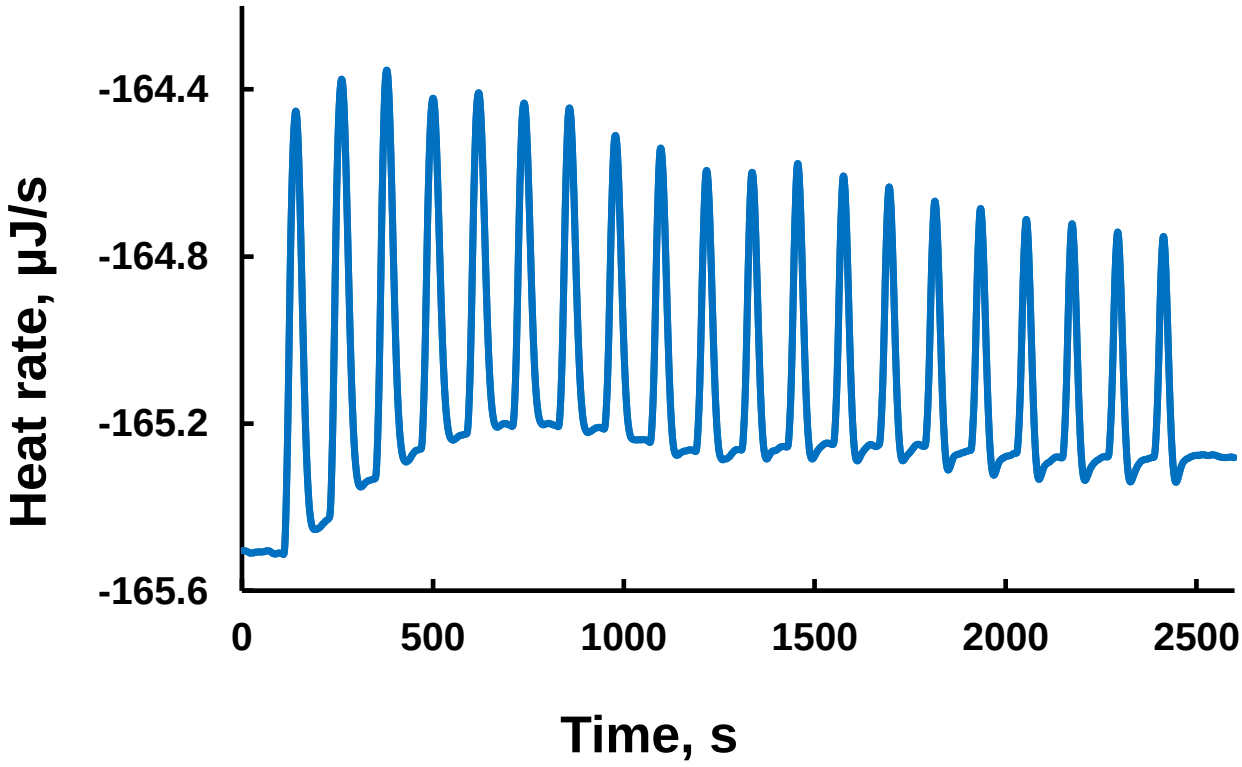

Figure 11: Calorimetric assay of oxalate oxidase using pyruvate as the substrate. 500 nM of oxalate oxidase (180 µL) in 25 mM sodium succinate (pH 4.0) was equilibrated at 25 ^{o}C. After 100 seconds, 2.5 µL of 150 mM pyruvate, pH 4.0 was injected every 120 seconds for 20 injections followed by a final 100 second period of data collection. The power required to maintain isothermal conditions is shown. Nanoanalyze (TA Instruments) was used to determine the kinetic parameters (Table 2) as described in the Materials and Methods section using an enthalpy value of -2.4 kJ/mol (data not shown).

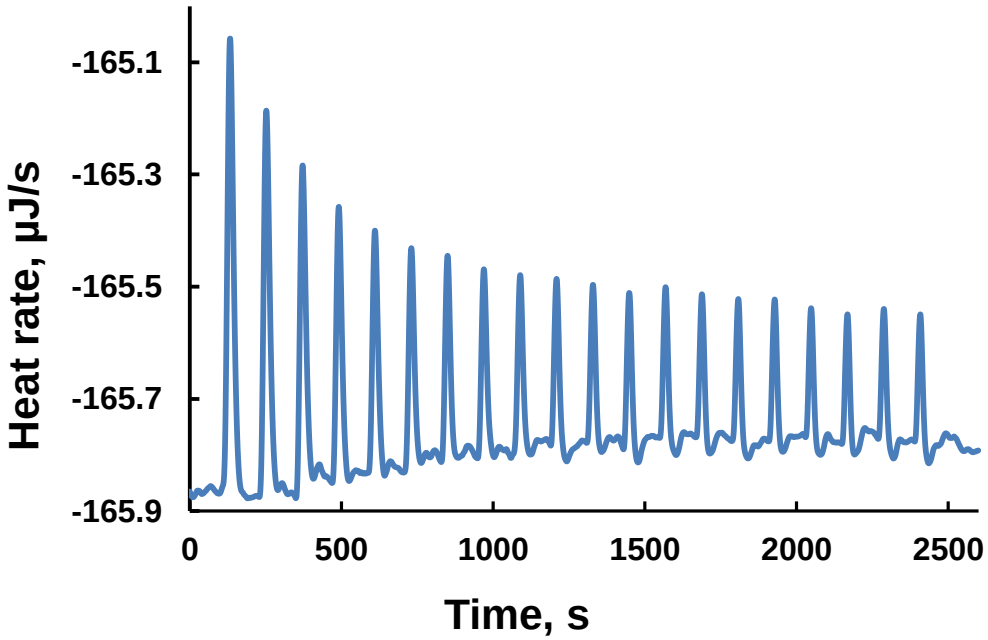

Figure 12: Calorimetric assay of oxalate oxidase using glyoxalate as the substrate. 500 nM of oxalate oxidase (180 µL) in 25 mM sodium succinate (pH 4.0) was equilibrated at 25 ºC. After 100 seconds, 2.5 µL of 100 mM glyoxalate, pH 4.0 was injected every 120 seconds for 20 injections followed by a final 100 second period of data collection. The power required to maintain isothermal conditions is shown. Nanoanalyze (TA Instruments) was used to determine the kinetic parameters (Table 2) as described in the Materials and Methods section using an enthalpy value of -3.8 kJ/mol (data not shown).

Table 2 shows the kinetic parameters of CsOxOx for the different carboxylic acids measured. The K_m for glyoxalate and malonate are similar, and an order of magnitude greater than that for oxalate or mesoxalate. The K_m for pyruvate is 40% that of glyoxalate, while the k_{cat} for pyruvate is nearly 3 times as larger than glyoxalate. The Michaelis-Menten fits for glyoxalate, pyruvate and malonate are shown in Figures 1, 2 and 3 in the Appendix. These ITC results have been published.[89]

Table 2: Steady-state kinetic parameters for the CsOxOx- catalyzed oxidation of alternative substrates measured by ITC.

Substrate	K_m, mM	k_{cat}, s^{-1}	Relative Activity, %
Oxalate	0.86 ± 0.1	15.6 ± 0.3	100
Mesoxalate	0.52 ± 0.1	9.9 ± 0.3	63.5
Glyoxalate	7.10 ± 0.1	0.46 ± 0.1	2.9
Malonate	6.42 ± 0.1	3.21 ± 0.1	20.5
Pyruvate	2.89 ± 0.1	1.25 ± 0.1	8.0
Malate	– nd[c]	nd[c]	<0.01

An Arrhenius plot was created to investigate the thermodynamic contribution of CsOxOx to catalysis of oxalate (Figure 13). The k_{cat} values were derived from the Michaelis-Menten fit at each temperature for oxalate (Figure 14, 15, & 16) and listed in Table 3. The k_{cat} value for 25 ^{o}C was used from Table 1. The energy of activation was calculated to be 45.89 kJ/mol (10.9 kcal/mol). The enthalpy of activation was determined to be 43.41 kJ/mol at 298 K. The Gibbs free energy was calculated to be 66.17 kJ/mol. The entropy of activation was calculated to be -22.76 kJ/mol K. The energy of activation for CsOxOx using oxalate was very similar to the energy of activation obtained for OxDC suggesting the mechanisms for oxalate oxidase and oxalate decarboxylase are similar.[82] The Gibbs free energy will be compared to other substrates and determine thermodynamic basis for the reactions with the alternative substrates. It will be very interesting to observe any changes in the thermodynamic parameters or reaction rates at certain temperatures to indicate a change in mechanisms.

Table 3: Turnover rates for the CsOxOx- catalyzed oxidation of oxalate by ITC at different temperatures.

k_{cat}, s^{-1}	Temperature (°C)
7.69	20
15.6	25
17.57	30
20.36	35

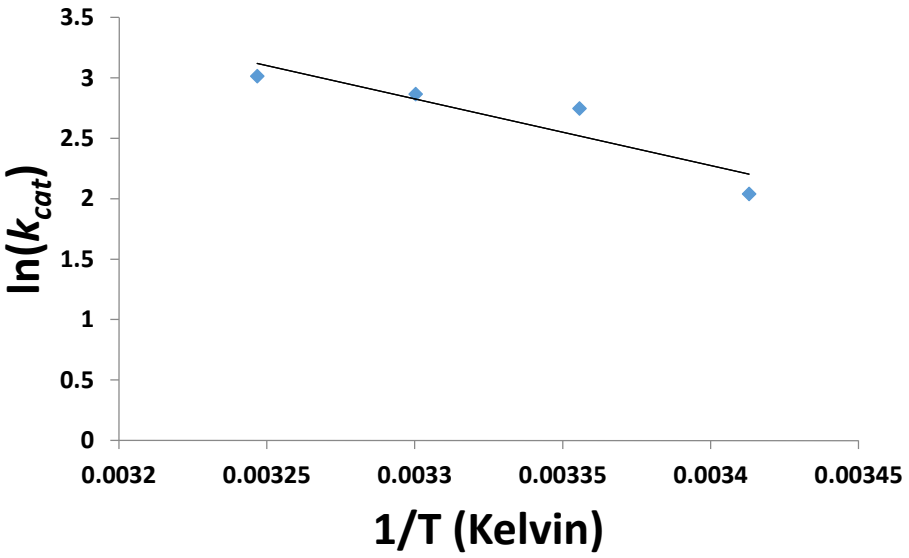

Figure 13: Arrhenius plot of the natural logarithm of k_{cat} versus the reciprocal of the absolute temperature.

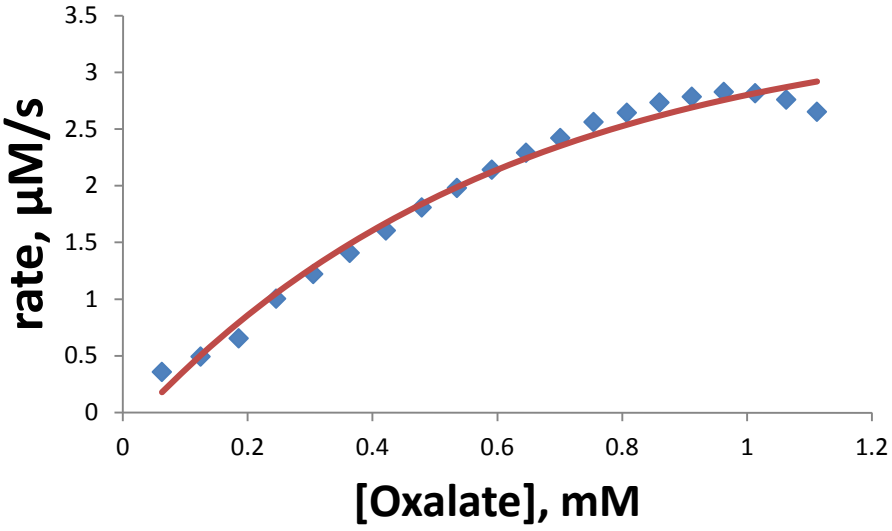

Figure 14: Rate extracted from the heat rate (data not shown) for oxalate is plotted against increasing concentration of oxalate corresponding to each injection at 20 ^{o}C. The kinetic values are obtained from the data fitted to the Michaelis-Menten equation.

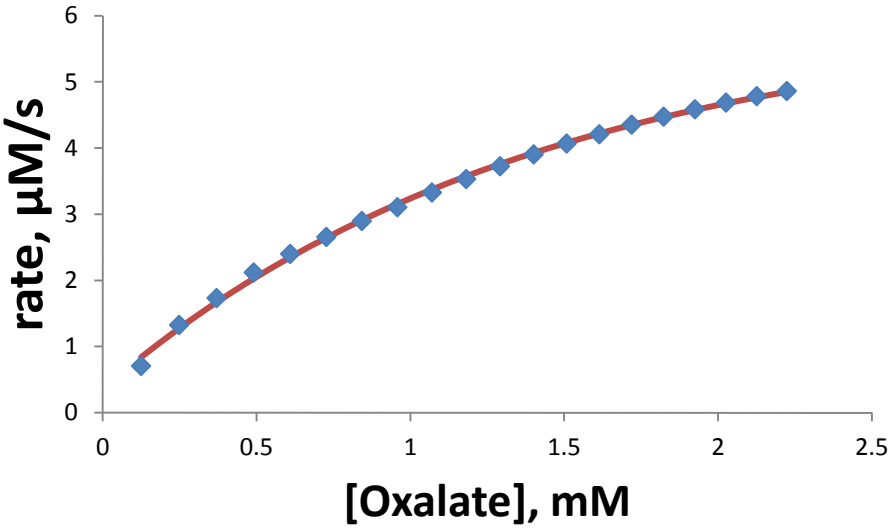

Figure 15: Rate extracted from the heat rate (data not shown) for oxalate is plotted against increasing concentration of oxalate corresponding to each injection at 30 ^{o}C. The kinetic values are obtained from the data fitted to the Michaelis-Menten equation.

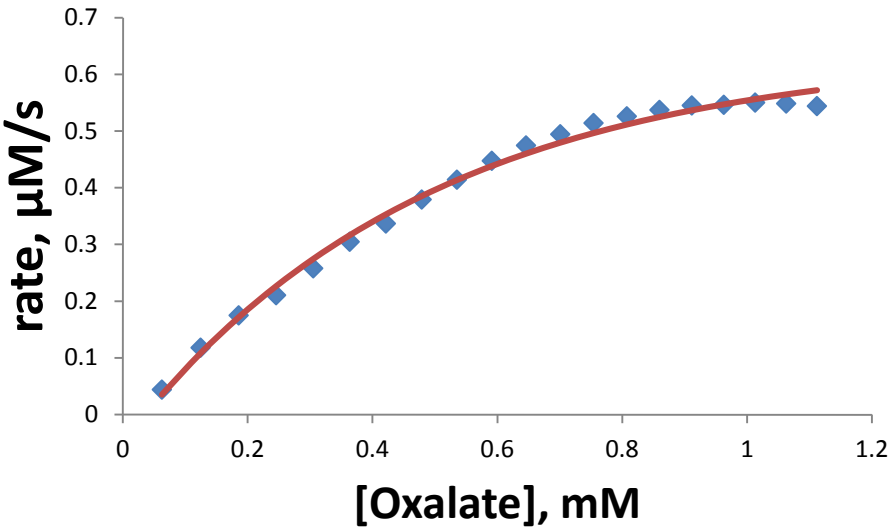

Figure 16: Rate extracted from the heat rate (data not shown) for oxalate is plotted against increasing concentration of oxalate corresponding to each injection 35 ºC. The kinetic values are obtained from the data fitted to the Michaelis-Menten equation.

Circular Dichroism

CD experiments were performed to monitor the secondary structures and thermodynamic parameters as a function of concentration, temperature and pH for wild type and different mutants. The CD spectra exhibited concentration dependence for wild-type CsOxOx, as the minima were shifted to the far UV upon dilution to lower concentrations (Figure 18). These results indicate that the oligomeric state of the enzyme varies enzyme concentration. CD Pro analysis of the contributions to each spectrum from the component secondary structural elements indicates the composition made mostly of beta strands (A1). The highest concentration tested (3.0 mg/ml) shows a minimum at 225 nm while 1.0 mg/ml spectrum shows a minimum at 212 nm.

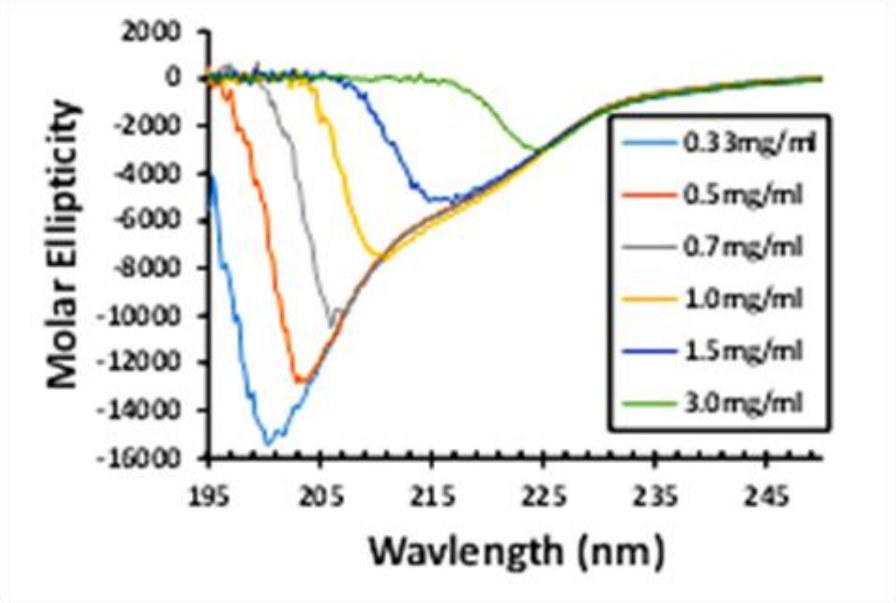

Figure 17: CD spectra for various concentrations of wild-type CsOxOx. All concentrations were performed in 25 mM phosphate buffer (pH 7.0): light blue, 0.33 mg/ml; orange, 0.5 mg/ml; grey, 0.7 mg/ml; yellow 1.0 mg/ml; dark blue, 1.5 mg/ml; green, 3.0 mg/ml.

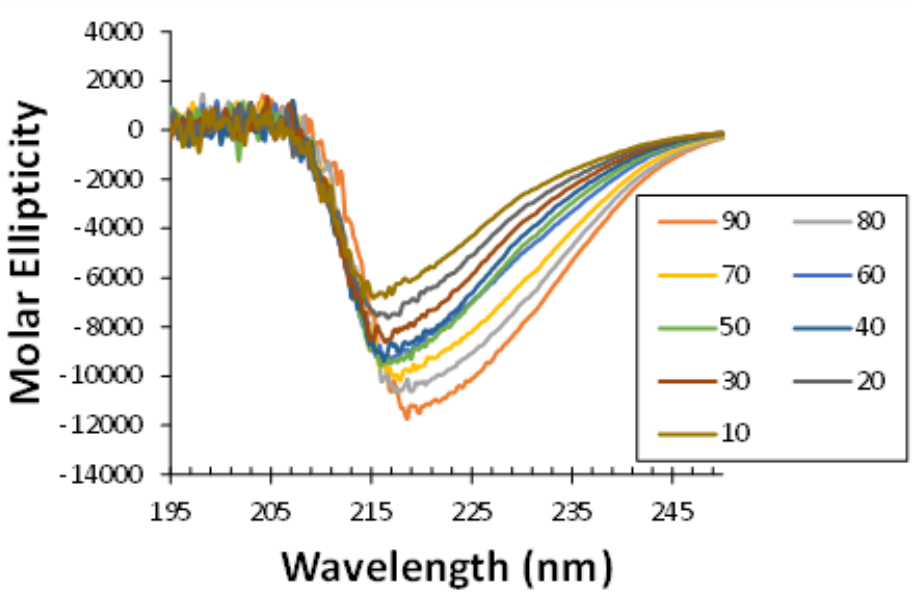

Figure 18: CD spectra of wild-type CsOxOx at different temperatures.0.68mg/ml sample was used in 25 mM potassium phosphate (pH 7.0): orange, 90 °C; grey, 80 °C; yellow, 70 °C; light blue, 60 °C; green, 50 °C; dark blue, 40 °C; brown, 30 °C; purple 20 °C; Tin, 10 °C.

The effect of temperature on the CD spectra of wild-type CsOxOx is shown in Figure 20. Spectra taken at higher temperatures exhibit a deeper minimum and a shift toward the near UV region. Most examples in the literature of the effect of temperature on the CD spectrum of proteins show a lesser degree of molar ellipticity upon increasing temperature.[90] There are, however, examples where the CD spectra display a greater degree of molar ellipticity as does CsOxOx (Figure 20). The melting curve for wild-type CsOxOx is shown in Figure 21. The spectrum exhibits a deeper ellipticity with increasing temperatures. The spectrum for the reverse scan overlaps with that of the forward scan indicating unfolding for wild-type CsOxOx is reversible.[91] Thermal denaturation analysis indicates the melting temperature, enthalpy and entropy of unfolding to be 54.52^{o}C, 631.72 kJ/mol, and 0.19 kJ/mol K, respectively.[92]

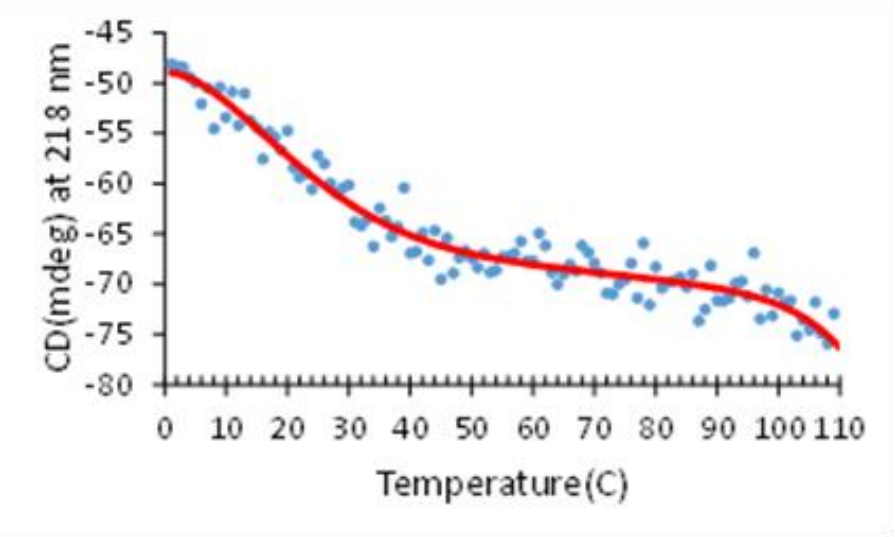

Figure 19: Thermal unfolding of wild-type CsOxOx monitored by CD at 218 nm wavelength in 25 mM sodium phosphate. Thermal denaturation was performed at temperatures 0-110 ^{o}C with 1 ^{o}C intervals.

Conclusions and Future Directions

This work has demonstrated the utility of using ITC to characterize the substrate promiscuity of CsOxOx. This work will be extended in the future to more potential substrates. Additional techniques will need to be employed to determine the reaction mechanisms and the products of the CsOxOx catalyzed reactions with these newly identified substrates. It is of interest to expand this work to characterize the substrate promiscuity of other oxalate degrading enzymes such as oxalate decarboxylase from *Bacillis subtilis* and oxalate oxidase form *Hordeum vulgare.* The utility of oxalate degrading enzymes for use in biofuel cells has stimulated interest in tailoring these enzymes for this purpose through the generation of mutant enzyme forms with a broader substrate range. ITC will be a valuable tool in the evaluation of engineered enzymes. Similarly, this work has shown that CD is a powerful tool that can be used to evaluate the overall protein structure of CsOxOx and the data collected will be used to compare with those of the engineered enzymes.

APPENDIX

Table 1: CDpro analysis of the distribution of secondary structural elements from the spectra in Figure 17.

	10ºC	**20ºC**	**30ºC**	**40ºC**	**50ºC**	**60ºC**	**70ºC**	**80ºC**	**90ºC**
Helixr	0.001	0.003	0.001	0	0	0	0	0	0.017
Helixd	0.034	0.041	0.032	0.042	0.034	0.032	0.035	0.036	0.028
Strandr	0.305	0.321	0.34	0.317	0.543	0.499	0.784	0.821	0.584
Strandd	0.136	0.134	0.13	0.132	0.119	0.116	0.182	0.114	0.154
T_m	0.216	0.203	0.221	0.207	0.129	0.151	0	0	0.063
Unorderd	0.309	0.298	0.276	0.302	0.176	0.202	0	0	0.152

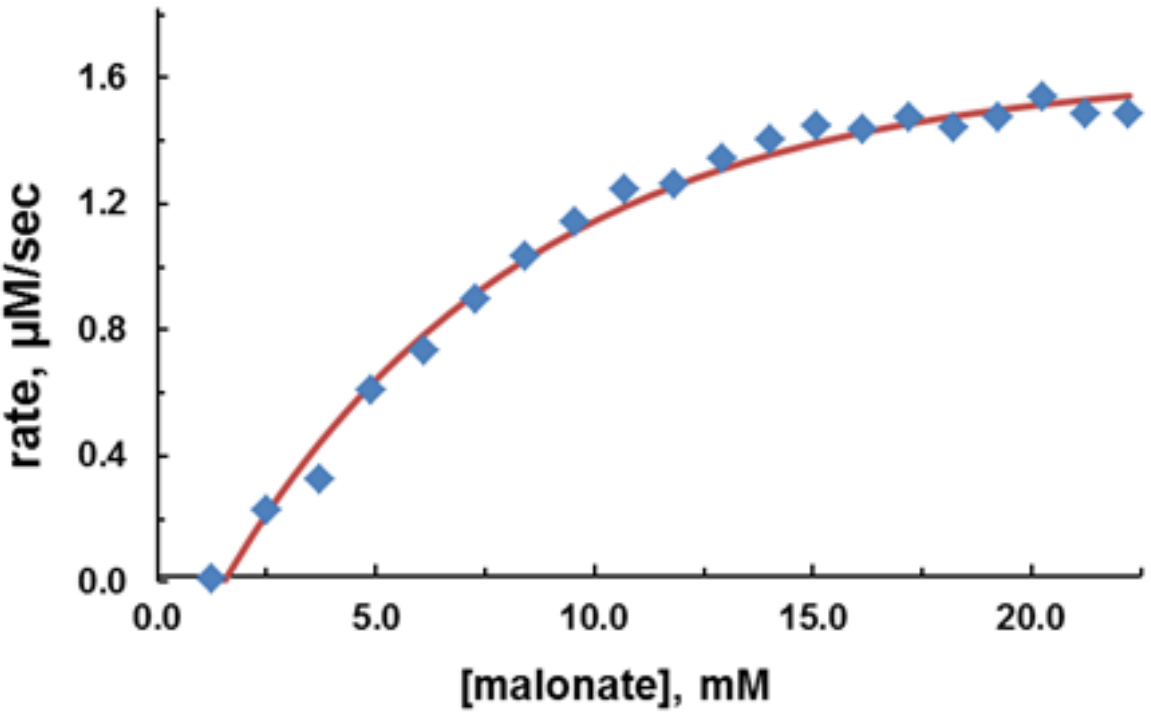

Figure 1: Rate extracted from the heat rate in Figure 10 for malonate is plotted against increasing concentration of malonate corresponding to each injection. The kinetic values are obtained from the data fitted to the Michaelis-Menten equation.

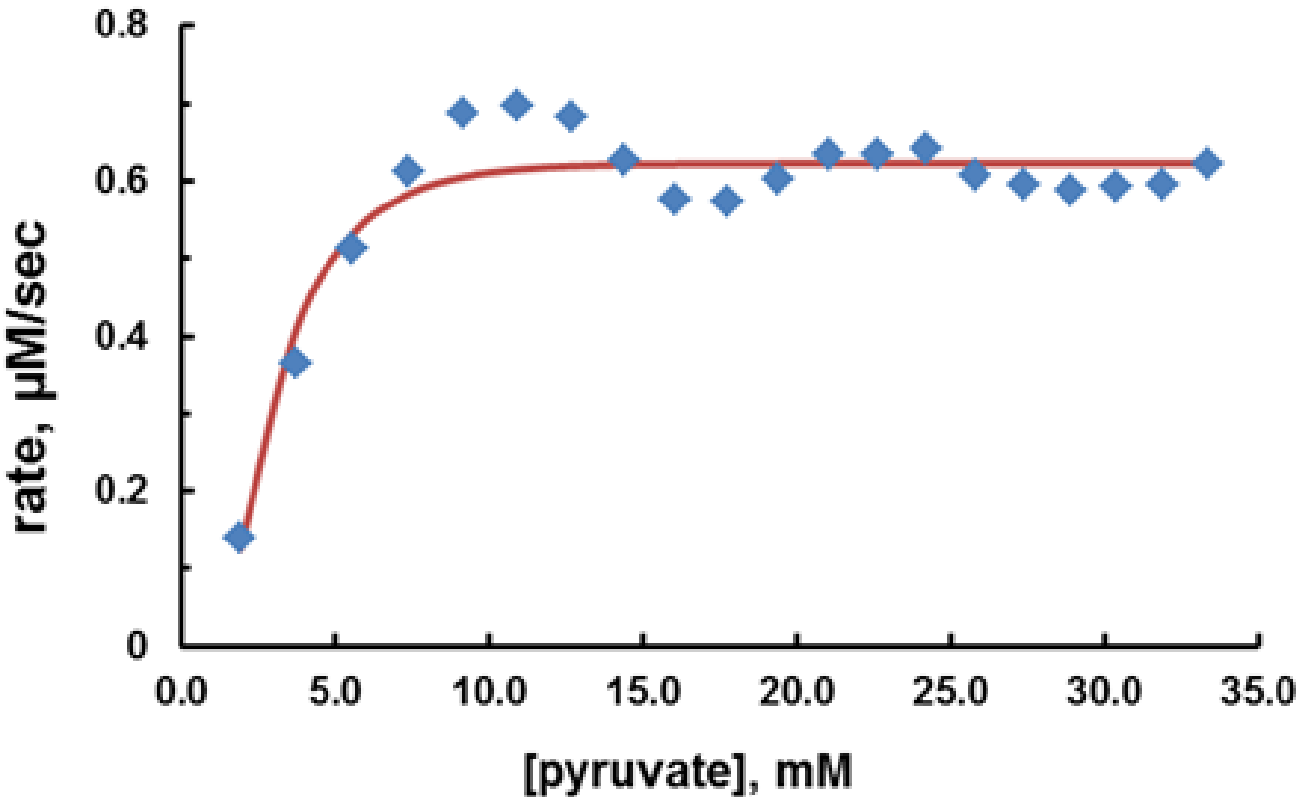

Figure 2: Rate extracted from the heat rate in Figure 11 for pyruvate is plotted against increasing concentration of pyruvate corresponding to each injection. The kinetic values are obtained from the data fitted to the Michaelis-Menten equation.

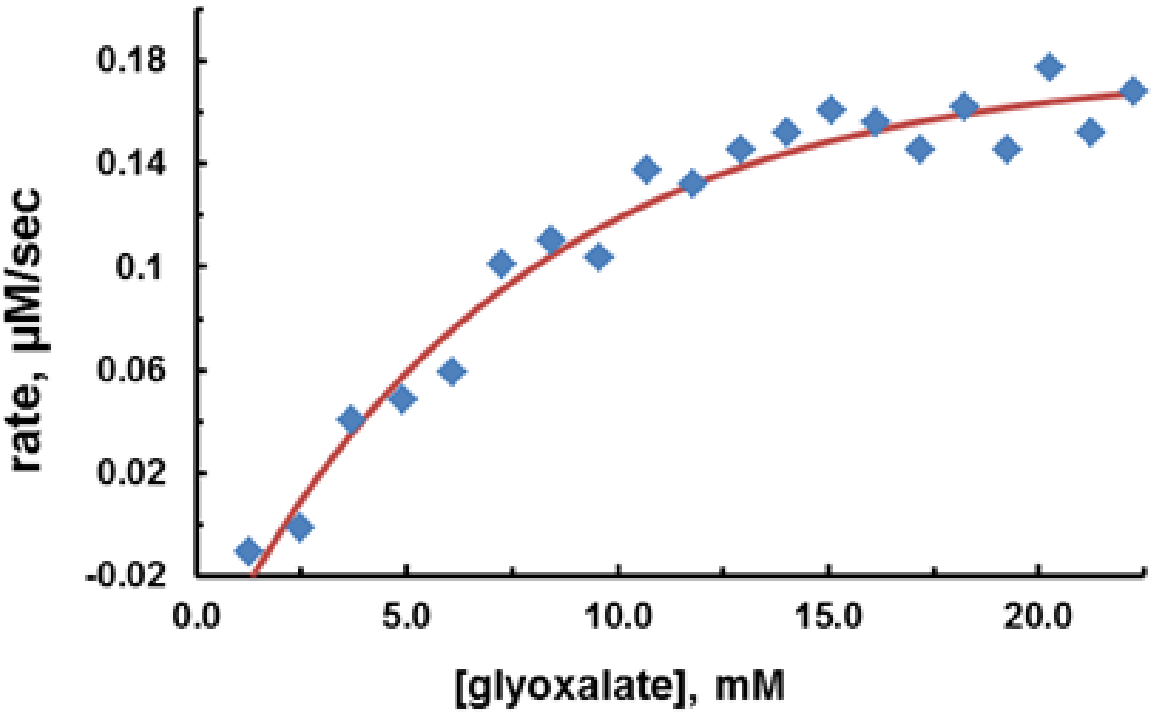

Figure 3: Rate extracted from the heat rate in Figure 12 for glyoxalate is plotted against increasing concentration of glyoxalate corresponding to each injection. The kinetic values are obtained from the data fitted to the Michaelis-Menten equation.

REFERENCES

1. White, D. J.,Jr A constant composition study of the kinetic of crystallization and demineralization of calcium oxalate: applications to renal stone disease, State University of New York at Buffalo, United States -- New York, 1982.

2. Franceschi, V. R.; Nakata, P. A. Calcium oxalate in plants: formation and function. *Annu.Rev.Plant Biol.* **2005***, 56*, 41-71.

3. Just, V. J.; Stevenson, C. E.; Bowater, L.; Tanner, A.; Lawson, D. M.; Bornemann, S. A closed conformation of Bacillus subtilis oxalate decarboxylase OxdC provides evidence for the true identity of the active site. *J. Biol. Chem.* **2004***, 279*, 19867-19874.

4. Kotsira, V. P.; Clonis, Y. D. Oxalate oxidase from barley roots: purification to homogeneity and study of some molecular, catalytic, and binding properties. *Arch. Biochem. Biophys.* **1997***, 340*, 239-249.

5. Shimazono, H. Oxalic acid decarboxylase, a new enzyme from the mycelium of wood destroying fungi. *The Journal of biochemistry* **1955***, 42*, 321-340.

6. Sahin, N. Oxalotrophic bacteria. *Res. Microbiol.* **2003***, 154*, 399-407.

7. Quayle, J. R. Carbon assimilation by Pseudomonas oxalaticus (OX1). 6. Reactions of oxalyl-coenzyme A. *Biochem. J.* **1963***, 87*, 368-373.

8. Reinhardt, L. A.; Svedruzic, D.; Chang, C. H.; Cleland, W. W.; Richards, N. G. Heavy Atom Isotope Effects on the Reaction Catalyzed by the Oxalate Decarboxylase from Bacillus s ubtilis. *J. Am. Chem. Soc.* **2003***, 125*, 1244-1252.

9. Dunwell, J. M.; Purvis, A.; Khuri, S. Cupins: the most functionally diverse protein superfamily? *Phytochemistry* **2004***, 65*, 7-17.

10. Tanner, A.; Bowater, L.; Fairhurst, S. A.; Bornemann, S. Oxalate decarboxylase requires manganese and dioxygen for activity. Overexpression and characterization of Bacillus subtilis YvrK and YoaN. *J. Biol. Chem.* **2001***, 276*, 43627-43634.

11. Gane, P. J.; Dunwell, J. M.; Warwickr, J. Modeling based on the structure of vicilins predicts a histidine cluster in the active site of oxalate oxidase. *J. Mol. Evol.* **1998***, 46*, 488-93.

12. Whittaker, M. M.; Whittaker, J. W. Characterization of recombinant barley oxalate oxidase expressed by Pichia pastoris. *JBIC Journal of Biological Inorganic Chemistry* **2002***, 7*, 136-145.

13. Scarpellini, M.; Gätjens, J.; Martin, O. J.; Kampf, J. W.; Sherman, S. E.; Pecoraro, V. L. Modeling the resting state of oxalate oxidase and oxalate decarboxylase enzymes. *Inorg. Chem.* **2008***, 47*, 3584-3593.

14. Woo, E.; Dunwell, J. M.; Goodenough, P. W.; Marvier, A. C.; Pickersgill, R. W. Germin is a manganese containing homohexamer with oxalate oxidase and superoxide dismutase activities. *Nature Structural & Molecular Biology* **2000***, 7*, 1036-1040.

15. Moomaw, E. W.; Hoffer, E.; Moussatche, P.; Salerno, J. C.; Grant, M.; Immelman, B.; Uberto, R.; Ozarowski, A.; Angerhofer, A. Kinetic and spectroscopic studies of bicupin oxalate oxidase and putative active site mutants. *PloS one* **2013***, 8*, e57933.

16. Escutia, M. R.; Bowater, L.; Edwards, A.; Bottrill, A. R.; Burrell, M. R.; Polanco, R.; Vicuna, R.; Bornemann, S. Cloning and sequencing of two Ceriporiopsis subvermispora bicupin oxalate oxidase allelic isoforms: implications for the reaction specificity of oxalate oxidases and decarboxylases. *Appl. Environ. Microbiol.* **2005***, 71*, 3608-3616.

17. Ruttimann-Johnson, C.; Salas, L.; Vicuna, R.; Kirk, T. K. Extracellular Enzyme Production and Synthetic Lignin Mineralization by Ceriporiopsis subvermispora. *Appl. Environ. Microbiol.* **1993***, 59*, 1792-1797.

18. Urzua, U.; Kersten, P. J.; Vicuna, R. Manganese Peroxidase-Dependent Oxidation of Glyoxylic and Oxalic Acids Synthesized by Ceriporiopsis subvermispora Produces Extracellular Hydrogen Peroxide. *Appl. Environ. Microbiol.* **1998***, 64*, 68-73.

19. Moussatche, P.; Angerhofer, A.; Imaram, W.; Hoffer, E.; Uberto, K.; Brooks, C.; Bruce, C.; Sledge, D.; Richards, N. G.; Moomaw, E. W. Characterization of Ceriporiopsis subvermispora bicupin oxalate oxidase expressed in Pichia pastoris. *Arch. Biochem. Biophys.* **2011***, 509*, 100-107.

20. Aguilar, C.; Urzúa, U.; Koenig, C.; Vicuña, R. Oxalate oxidase from Ceriporiopsis subvermispora: biochemical and cytochemical studies. *Arch. Biochem. Biophys.* **1999***, 366*, 275-282.

21. Moomaw, E. W.; Uberto, R.; Tu, C. Membrane inlet mass spectrometry reveals that Ceriporiopsis subvermispora bicupin oxalate oxidase is inhibited by nitric oxide. *Biochem. Biophys. Res. Commun.* **2014***, 450*, 750-754.

22. Woo, E.; Dunwell, J. M.; Goodenough, P. W.; Pickersgill, R. W. Barley oxalate oxidase is a hexameric protein related to seed storage proteins: evidence from X-ray crystallography. *FEBS Lett.* **1998***, 437*, 87-90.

23. Dumas, B.; Sailland, A.; Cheviet, J. P.; Freyssinet, G.; Pallett, K. Identification of barley oxalate oxidase as a germin-like protein. *C. R. Acad. Sci. III.* **1993***, 316*, 793-798.

24. Requena, L.; Bornemann, S. Barley (Hordeum vulgare) oxalate oxidase is a manganese-containing enzyme. *Biochem. J.* **1999***, 343*, 185-190.

25. Opaleye, O.; Rose, R. S.; Whittaker, M. M.; Woo, E. J.; Whittaker, J. W.; Pickersgill, R. W. Structural and spectroscopic studies shed light on the mechanism of oxalate oxidase. *J. Biol. Chem.* **2006***, 281*, 6428-6433.

26. Whittaker, M. M.; Whittaker, J. W. Characterization of recombinant barley oxalate oxidase expressed by Pichia pastoris. *JBIC Journal of Biological Inorganic Chemistry* **2002***, 7*, 136-145.

27. Zhou, F.; Zhang, Z.; Gregersen, P. L.; Mikkelsen, J. D.; de Neergaard, E.; Collinge, D. B.; Thordal-Christensen, H. Molecular characterization of the oxalate oxidase involved in the response of barley to the powdery mildew fungus. *Plant Physiol.* **1998***, 117*, 33-41.

28. Livingstone, D. M.; Hampton, J. L.; Phipps, P. M.; Grabau, E. A. Enhancing resistance to Sclerotinia minor in peanut by expressing a barley oxalate oxidase gene. *Plant Physiol.* **2005***, 137*, 1354-1362.

29. Tanner, A.; Bornemann, S. Bacillus subtilis YvrK is an acid-induced oxalate decarboxylase. *J. Bacteriol.* **2000***, 182*, 5271-5273.

30. Anand, R.; Dorrestein, P. C.; Kinsland, C.; Begley, T. P.; Ealick, S. E. Structure of oxalate decarboxylase from Bacillus subtilis at 1.75 Å resolution. *Biochemistry (N. Y.)* **2002***, 41*, 7659-7669.

31. Angerhofer, A.; Moomaw, E. W.; García-Rubio, I.; Ozarowski, A.; Krzystek, J.; Weber, R. T.; Richards, N. G. Multifrequency EPR studies on the Mn (II) centers of oxalate decarboxylase. *The Journal of Physical Chemistry B* **2007***, 111*, 5043-5046.

32. Reinhardt, L. A.; Svedruzic, D.; Chang, C. H.; Cleland, W. W.; Richards, N. G. Heavy Atom Isotope Effects on the Reaction Catalyzed by the Oxalate Decarboxylase from Bacillus s ubtilis. *J. Am. Chem. Soc.* **2003***, 125*, 1244-1252.

33. Just, V. J.; Stevenson, C. E.; Bowater, L.; Tanner, A.; Lawson, D. M.; Bornemann, S. A closed conformation of Bacillus subtilis oxalate decarboxylase OxdC provides evidence for the true identity of the active site. *J. Biol. Chem.* **2004***, 279*, 19867-19874.

34. Just, V.; Burrell, M.; Bowater, L.; McRobbie, I.; Stevenson, C.; Lawson, D.; Bornemann, S. The identity of the active site of oxalate decarboxylase and the importance of the stability of active-site lid conformations1. *Biochem. J.* **2007***, 407*, 397-406.

35. Svedružić, D.; Liu, Y.; Reinhardt, L. A.; Wroclawska, E.; Cleland, W. W.; Richards, N. G. Investigating the roles of putative active site residues in the oxalate decarboxylase from Bacillus subtilis. *Arch. Biochem. Biophys.* **2007***, 464*, 36-47.

36. Tanner, A.; Bowater, L.; Fairhurst, S. A.; Bornemann, S. Oxalate decarboxylase requires manganese and dioxygen for activity. Overexpression and characterization of Bacillus subtilis YvrK and YoaN. *J. Biol. Chem.* **2001***, 276*, 43627-43634.

37. Burrell, M. R.; Just, V. J.; Bowater, L.; Fairhurst, S. A.; Requena, L.; Lawson, D. M.; Bornemann, S. Oxalate decarboxylase and oxalate oxidase activities can be interchanged with a specificity switch of up to 282 000 by mutating an active site lid. *Biochemistry (N. Y.)* **2007***, 46*, 12327-12336.

38. Magro, P.; Marciano, P.; Di Lenna, P. Enzymatic oxalate decarboxylation in isolates of Sclerotinia sclerotiorum. *FEMS Microbiol. Lett.* **1988***, 49*, 49-52.

39. Williams, B.; Kabbage, M.; Kim, H.; Britt, R.; Dickman, M. B. Tipping the balance: Sclerotinia sclerotiorum secreted oxalic acid suppresses host defenses by manipulating the host redox environment. *PLoS Pathog* **2011***, 7*, e1002107.

40. Liang, X.; Moomaw, E. W.; Rollins, J. A. Fungal oxalate decarboxylase activity contributes to Sclerotinia sclerotiorum early infection by affecting both compound appressoria development and function. *Molecular plant pathology* **2015**.

41. Zerwekh, J. E.; Drake, E.; Gregory, J.; Griffith, D.; Hofmann, A. F.; Menon, M.; Pak, C. Y. Assay of urinary oxalate: six methodologies compared. *Clin. Chem.* **1983***, 29*, 1977-1980.

42. Hesse, A.; Bongartz, D.; Heynck, H.; Berg, W. Measurement of urinary oxalic acid: a comparison of five methods. *Clin. Biochem.* **1996***, 29*, 467-472.

43. Massey, L. K.; Roman-Smith, H.; Sutton, R. A. Effect of dietary oxalate and calcium on urinary oxalate and risk of formation of calcium oxalate kidney stones. *J. Am. Diet. Assoc.* **1993***, 93*, 901-906.

44. Watterson, J. D.; Cadieux, P. A.; Beiko, D. T.; Cook, A. J.; Burton, J. P.; Harbottle, R. R.; Lee, C.; Rowe, E.; Sidhu, H.; Reid, G. Oxalate-degrading enzymes from Oxalobacter formigenes: a novel device coating to reduce urinary tract biomaterial-related encrustation. *Journal of endourology* **2003***, 17*, 269-274.

45. Hoppe, B.; von Unruh, G.; Laube, N.; Hesse, A.; Sidhu, H. Oxalate degrading bacteria: new treatment option for patients with primary and secondary hyperoxaluria? *Urol. Res.* **2005***, 33*, 372-375.

46. Carrillo, M. G. C.; Goodwin, P. H.; Leach, J. E.; Leung, H.; Cruz, C. M. V. Phylogenomic relationships of rice oxalate oxidases to the cupin superfamily and their association with disease resistance QTL. *Rice* **2009***, 2*, 67-79.

47. Thompson, C.; Dunwell, J.; Johnstone, C.; Lay, V.; Ray, J.; Schmitt, M.; Watson, H.; Nisbet, G. Degradation of oxalic acid by transgenic oilseed rape plants expressing oxalate oxidase. In *The Methodology of Plant Genetic Manipulation: Criteria for Decision Making*Springer: 1995; pp 169-172.

48. Godoy, G.; Steadman, J.; Dickman, M.; Dam, R. Use of mutants to demonstrate the role of oxalic acid in pathogenicity of Sclerotinia sclerotiorum on Phaseolus vulgaris. *Physiol. Mol. Plant Pathol.* **1990***, 37*, 179-191.

49. Thompson, C.; Dunwell, J.; Johnstone, C.; Lay, V.; Ray, J.; Schmitt, M.; Watson, H.; Nisbet, G. Degradation of oxalic acid by transgenic oilseed rape plants expressing oxalate oxidase. In *The Methodology of Plant Genetic Manipulation: Criteria for Decision Making*Springer: 1995; pp 169-172.

50. Sjöde, A.; Winestrand, S.; Nilvebrant, N.; Jönsson, L. J. Enzyme-based control of oxalic acid in the pulp and paper industry. *Enzyme Microb. Technol.* **2008***, 43*, 78-83.

51. Asgher, M.; Bhatti, H. N.; Ashraf, M.; Legge, R. L. Recent developments in biodegradation of industrial pollutants by white rot fungi and their enzyme system. *Biodegradation* **2008***, 19*, 771-783.

52. Reid, I. D.; Paice, M. G. Biological bleaching of kraft pulps by white-rot fungi and their enzymes. *FEMS Microbiol. Rev.* **1994***, 13*, 369-376.

53. Leonowicz, A.; Matuszewska, A.; Luterek, J.; Ziegenhagen, D.; Wojtaś-Wasilewska, M.; Cho, N.; Hofrichter, M.; Rogalski, J. Biodegradation of lignin by white rot fungi. *Fungal genetics and biology* **1999***, 27*, 175-185.

54. Paice, M. G.; Reid, I. D.; Bourbonnais, R.; Archibald, F. S.; Jurasek, L. Manganese Peroxidase, Produced by Trametes versicolor during Pulp Bleaching, Demethylates and Delignifies Kraft Pulp. *Appl. Environ. Microbiol.* **1993***, 59*, 260-265.

55. Arechederra, R.; Minteer, S. Complete oxidation of glycerol in an enzymatic biofuel cell. *Fuel Cells* **2009***, 9*, 63-69.

56. Ivanov, I.; Vidaković-Koch, T.; Sundmacher, K. Recent advances in enzymatic fuel cells: experiments and modeling. *Energies* **2010***, 3*, 803-846.

57. Hickey, D. P.; McCammant, M. S.; Giroud, F.; Sigman, M. S.; Minteer, S. D. Hybrid Enzymatic and Organic Electrocatalytic Cascade for the Complete Oxidation of Glycerol. *J. Am. Chem. Soc.* **2014***, 136*, 15917-15920.

58. Osman, M.; Shah, A.; Walsh, F. Recent progress and continuing challenges in bio-fuel cells. Part I: Enzymatic cells. *Biosensors and Bioelectronics* **2011***, 26*, 3087-3102.

59. Rasmussen, M.; Abdellaoui, S.; Minteer, S. D. Enzymatic biofuel cells: 30 years of critical advancements. *Biosensors and Bioelectronics* **2016***, 76*, 91-102.

60. Minteer, S. D.; Liaw, B. Y.; Cooney, M. J. Enzyme-based biofuel cells. *Curr. Opin. Biotechnol.* **2007***, 18*, 228-234.

61. Marcus, R. A.; Sutin, N. Electron transfers in chemistry and biology. *Biochimica et Biophysica Acta (BBA)-Reviews on Bioenergetics* **1985***, 811*, 265-322.

62. Mateo, C.; Palomo, J. M.; Fernandez-Lorente, G.; Guisan, J. M.; Fernandez-Lafuente, R. Improvement of enzyme activity, stability and selectivity via immobilization techniques. *Enzyme Microb. Technol.* **2007***, 40*, 1451-1463.

63. Hickey, D. P.; McCammant, M. S.; Giroud, F.; Sigman, M. S.; Minteer, S. D. Hybrid Enzymatic and Organic Electrocatalytic Cascade for the Complete Oxidation of Glycerol. *J. Am. Chem. Soc.* **2014***, 136*, 15917-15920.

64. Abdellaoui, S.; Hickey, D. P.; Stephens, A. R.; Minteer, S. D. Recombinant oxalate decarboxylase: enhancement of a hybrid catalytic cascade for the complete electro-oxidation of glycerol. *Chemical Communications* **2015***, 51*, 14330-14333.

65. Güven, G.; Prodanovic, R.; Schwaneberg, U. Protein engineering–an option for enzymatic biofuel cell design. *Electroanalysis* **2010***, 22*, 765-775.

66. Copley, S. D. An evolutionary biochemist's perspective on promiscuity. *Trends Biochem. Sci.* **2015***, 40*, 72-78.

67. Bhat, V.; Olenick, M. B.; Schuchardt, B. J.; Mikles, D. C.; McDonald, C. B.; Farooq, A. Biophysical basis of the promiscuous binding of B-cell lymphoma protein 2 apoptotic repressor to BH3 ligands. *Journal of Molecular Recognition* **2013***, 26*, 501-513.

68. Roodveldt, C.; Tawfik, D. S. Shared promiscuous activities and evolutionary features in various members of the amidohydrolase superfamily. *Biochemistry (N. Y.)* **2005***, 44*, 12728-12736.

69. Honaker, M. T.; Acchione, M.; Zhang, W.; Mannervik, B.; Atkins, W. M. Enzymatic detoxication, conformational selection, and the role of molten globule active sites. *J. Biol. Chem.* **2013***, 288*, 18599-18611.

70. Jensen, R. A. Enzyme recruitment in evolution of new function. *Annual Reviews in Microbiology* **1976***, 30*, 409-425.

71. Gerlt, J. A.; Babbitt, P. C.; Rayment, I. Divergent evolution in the enolase superfamily: the interplay of mechanism and specificity. *Arch. Biochem. Biophys.* **2005***, 433*, 59-70.

72. Bornscheuer, U.; Huisman, G.; Kazlauskas, R.; Lutz, S.; Moore, J.; Robins, K. Engineering the third wave of biocatalysis. *Nature* **2012***, 485*, 185-194.

73. Tokuriki, N.; Tawfik, D. S. Protein dynamism and evolvability. *Science* **2009***, 324*, 203-207.

74. Villiers, B. R.; Hollfelder, F. Mapping the limits of substrate specificity of the adenylation domain of TycA. *ChemBioChem* **2009***, 10*, 671-682.

75. van Loo, B.; Jonas, S.; Babtie, A. C.; Benjdia, A.; Berteau, O.; Hyvonen, M.; Hollfelder, F. An efficient, multiply promiscuous hydrolase in the alkaline phosphatase superfamily. *Proc. Natl. Acad. Sci. U. S. A.* **2010***, 107*, 2740-2745.

76. Jonas, S.; Hollfelder, F. Mapping catalytic promiscuity in the alkaline phosphatase superfamily. *Pure and Applied Chemistry* **2009***, 81*, 731-742.

77. Morin, P. E.; Freire, E. Direct calorimetric analysis of the enzymic activity of yeast cytochrome c oxidase. *Biochemistry (N. Y.)* **1991***, 30*, 8494-8500.

78. Todd, M. J.; Gomez, J. Enzyme kinetics determined using calorimetry: a general assay for enzyme activity? *Anal. Biochem.* **2001***, 296*, 179-187.

79. Sharma, G.; First, E. A. Thermodynamic analysis reveals a temperature-dependent change in the catalytic mechanism of bacillus stearothermophilus tyrosyl-tRNA synthetase. *J. Biol. Chem.* **2009***, 284*, 4179-4190.

80. Andújar-Sánchez, M.; Las Heras-Vázquez, F. J.; Clemente-Jiménez, J. M.; Martínez-Rodríguez, S.; Camara-Artigas, A.; Rodríguez-Vico, F.; Jara-Pérez, V. Enzymatic activity assay of d-hydantoinase by isothermal titration calorimetry. Determination of the thermodynamic activation parameters for the hydrolysis of several substrates. *J. Biochem. Biophys. Methods* **2006***, 67*, 57-66.

81. Labrou, N. E.; Kotzia, G. A.; Clonis, Y. D. Engineering the xenobiotic substrate specificity of maize glutathione S-transferase I. *Protein Eng. Des. Sel.* **2004***, 17*, 741-748.

82. Molina, L.; Goodall, T.; Twahir, U.; Moomaw, E.; Angerhofer, A. Real-Time kinetic studies of Bacillus subtilis oxalate decarboxylase and Ceriporiopsis subvermispora oxalate oxidase using a luminescent oxygen sensor. *Journal of Biochemical Technology* **2015***, 5*, 826-831.

83. Kelly, S. M.; Price, N. C. The use of circular dichroism in the investigation of protein structure and function. *Current protein and peptide science* **2000***, 1*, 349-384.

84. Greenfield, N. J. Applications of circular dichroism in protein and peptide analysis. *TrAC Trends in Analytical Chemistry* **1999***, 18*, 236-244.

85. Goyal, M.; Chaudhuri, T. K.; Kuwajima, K. Irreversible Denaturation of Maltodextrin Glucosidase Studied by Differential Scanning Calorimetry, Circular Dichroism, and Turbidity Measurements. *PloS one* **2014***, 9*, e115877.

86. Nisha, M.; Satyanarayana, T. Characteristics of thermostable amylopullulanase of Geobacillus thermoleovorans and its truncated variants. *Int. J. Biol. Macromol.* **2015***, 76*, 279-291.

87. Lowry, O. H.; Rosebrough, N. J.; Farr, A. L.; Randall, R. J. Protein measurement with the Folin phenol reagent. *J. Biol. Chem.* **1951***, 193*, 265-275.

88. Rudrappa, T.; Choi, Y. S.; Levia, D. F.; Legates, D. R.; Lee, K. H.; Bais, H. P. Phragmites australis root secreted phytotoxin undergoes photo-degradation to execute severe phytotoxicity. *Plant signaling & behavior* **2009***, 4*, 506-513.

89. Rana, H.; Moussatche, P.; Rocha, L. S.; Abdellaoui, S.; Minteer, S. D.; Moomaw, E. W. Isothermal titration calorimetry uncovers substrate promiscuity of bicupin oxalate oxidase from Ceriporiopsis subvermispora. *Biochemistry and Biophysics Reports* **2016***, 5*, 396-400.

90. Greenfield, N. J. Using circular dichroism collected as a function of temperature to determine the thermodynamics of protein unfolding and binding interactions. *Nature protocols* **2006***, 1*, 2527-2535.

91. Angerhofer, A.; Ozarowski, A.; Hoffer, E.; Grant, M.; Immelman, B.; Moomaw, E. Kinetic and Spectroscopic Characterization of Bicupin Oxalate Oxidase and Putative Active Site Mutants.

92. Baid, R.; Upadhyay, A. K.; Shinohara, T.; Kompella, U. B. Biosynthesis, characterization, and efficacy in retinal degenerative diseases of lens epithelium-derived growth factor fragment (LEDGF1-326), a novel therapeutic protein. *J. Biol. Chem.* **2013***, 288*, 17372-17383.